UPPER CRUSTAL STRUCTURE OF THE NORTHERN WASATCH FRONT, UTAH, FROM SEISMIC REFLECTION AND GRAVITY DATA

by

Bernard R. McNeil

and

Robert B. Smith

Department of Geology and Geophysics
University of Utah
Salt Lake City, Utah 84112

THE PUBLICATION OF THIS PAPER
IS MADE POSSIBLE WITH MINERAL LEASE FUNDS

ABSTRACT

Three data sets are used in this study: 1) seismic reflection profiles supplied by Elf Aquitaine Petroleum; 2) the complete Bouguer anomaly gravity data for the area; and 3) geophysical well logs from the Utah Oil and Gas Commission. Depth-to-basement values determined from the interpretation of seismic profiles and a density contrast of -0.53 g/cc calculated from the density well logs were used as constraints for a three-dimensional gravity inversion using a nonlinear weighted and damped least squares method. A basin model was generated by contouring the depths determined from the seismic profiles and gravity inversion results.

The depth-to-basement contour map produced in this study shows basin depths and geometries which closely match (differ by < 15% in all cases) the four two-dimensional profiles produced by other investigators. The basin geometry elucidated by the depth-to-basement contour map implies the segments of the Wasatch fault in the study area are affected by Early and Pre-Cenozoic structures, i.e., the Absaroka ramp-anticline, the Salt Lake salient and the thrust sheets north of Ogden. The depth-to-basement model produced in this study shows a depression in the basin between Ogden and Brigham City. If this depression is real, the notion of persistent segment boundaries in this area has to be rethought, because the southern portion of the deep spot is located at a segment boundary. Finally, the geometry of the Weber Basin is significantly different than the geometry of the Great Salt Lake Basin.

CONTENTS

LIST OF FIGURES

ACKNOWLEDGMENTS

INTRODUCTION

The Wasatch Front extends from the south end of Utah valley in central Utah northward to Idaho, and is considered the tectonic boundary between the Basin-Range province and the Rocky Mountains to the north and the Colorado Plateau to the south. The Wasatch fault zone which trends 370 km north-south along the front is one of the largest normal fault systems in the United States and bounds the Wasatch Range which rises 1.5 km above the valley floor. This area has been the focus of recent studies aimed at delineation of earthquake hazards and understanding the general seismotectonics of the region. Studies have ranged from fault segment mapping (Schwartz and Coppersmith, 1984; Machette, Personius, Nelson, Schwartz and Lund, 1991) to determination of strain rate (Snay, Smith and Soler, 1984), to delineating the regional seismicity (Arabasz, Pechmann and Brown, 1987).

Most basin studies, to determine basin geometry, have been motivated by the search for natural resources such as ore deposits, oil and natural gas. A few basin studies have been conducted to obtain information on ground water systems, or for earthquake hazards analyses in populated areas. This study is motivated by two objectives: 1) to determine the geometry of the basin west of the Wasatch fault from Bountiful northward to Brigham City; and 2) to produce useful information about the Wasatch fault geometry and provide earthquake hazards investigators with a basin model for use in site amplification studies. The study area is shown in Figure 1 and will hereafter be referred to as the Weber Basin study area.

Three types of data were used in this study: 1) seismic reflection profiles provided by Elf Aquitaine Petroleum; 2) the complete Bouguer anomaly (CBA) gravity
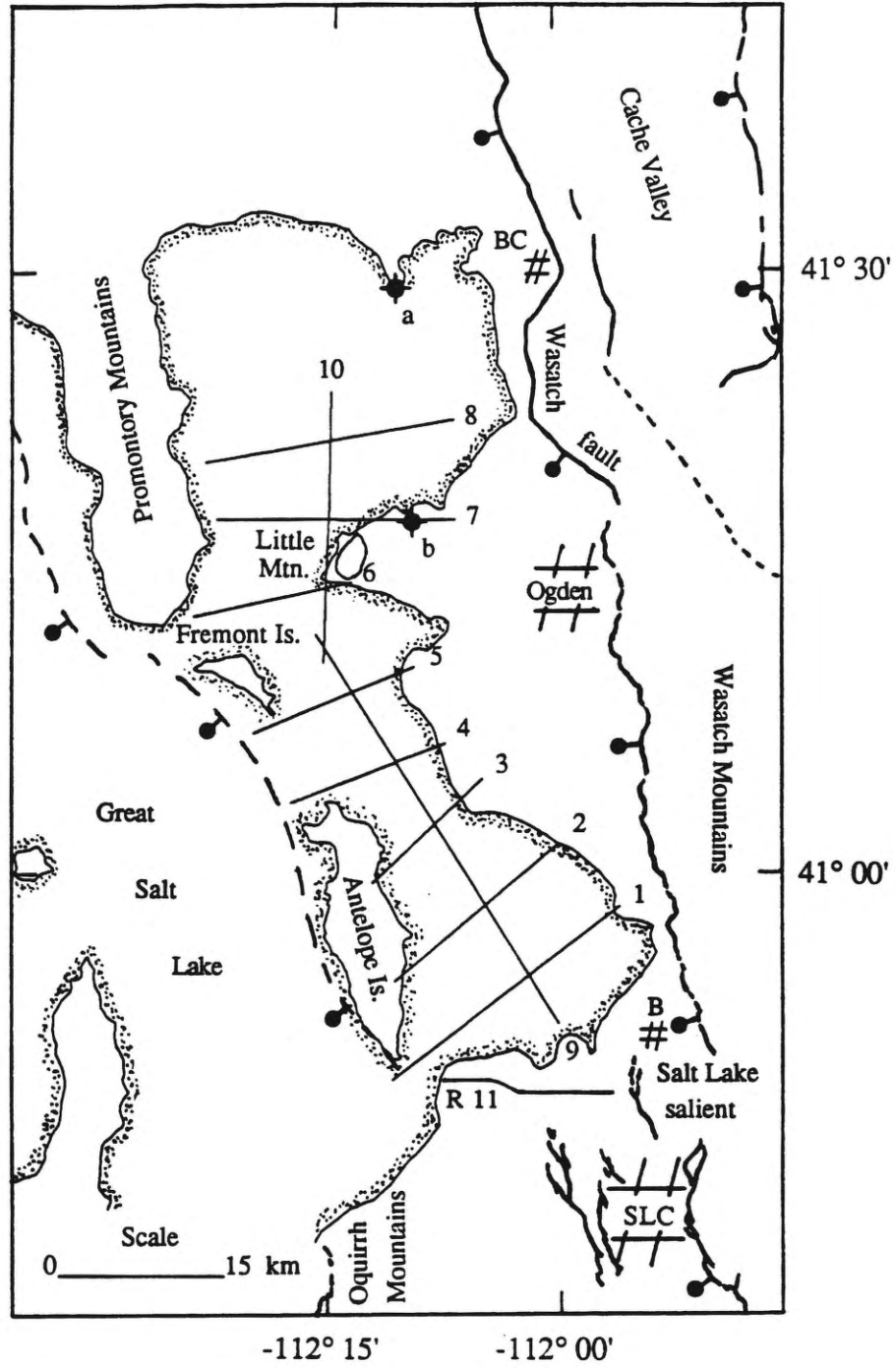
Figure 1. Map showing the location of the study area along with prominent regional features. Seismic reflection profiles are labelled 1–10 and R 11, wells are labelled "a" and "b", SLC = Salt Lake City, B = Bountiful, BC = Brigham City.

data compiled by Cook, Bankey, Mabey and DePangher (1989); and 3) geophysical well logs on file at the Utah Oil and Gas Commission. Depth-to-basement values determined from the interpretation of seismic profiles and a density contrast of -0.53 g/cc calculated from the density well logs were used as constraints for a three-dimensional gravity inversion; a nonlinear weighted and damped least squares method is used to determine the three-dimensional geometry of the Weber Basin. A basin model was generated by contouring the depths determined from the seismic profiles and gravity inversion results.

Previous Work

Though numerous studies have been conducted along the Weber Basin, no three-dimensional gravity modeling has been attempted. All previous modeling work has been restricted to two-dimensional gravity studies. Glenn, Chapman, Foley, Capuano, Cole, Sibbett, and Ward (1980) conducted a geothermal study at Hill Air Force Base which included seismic reflection, gravity and heat flow studies. The objectives of both the seismic reflection and gravity studies were to determine the basin and fault geometries. Zoback (1983) compiled 22 two-dimensional gravity profiles produced by forward modeling, three of which are located in this study area. Zoback (1983) used these profiles along with seismic reflection, contoured CBA gravity, and well data to study the Cenozoic tectonics and structure along the Wasatch fault. The maximum basin depths shown by Zoback (1983) for this study area ranged from 1.8 to 2.6 km. Zoback's (1983) study is of a considerably broader scope than this study. Wilson, Saugy and Zimmermann (1986) interpreted four seismic reflection profiles from Elf Aquitaine Petroleum, to determine basin geometry on the east side of the Great Salt Lake. They showed maximum basin depths of between 2.1 to 4.0 km for the Weber basin. Lambert and West (1989) conducted a continuous seismic profiling study east of

Antelope and Fremont islands to determine the geometry of the basin for use in ground water studies. The depth-to-basement map produced in this study shows maximum basement depths of > 0.5 km over their area of interest. The results of this study are compared with these investigators' results.

Two investigations of nearby basins were carried out by Viveiros (1986) and Radkins (1990). Viveiros (1986) reprocessed and interpreted several seismic reflection profiles, donated by Amoco Oil Co., to determine the geometry of the basin on the west side of the Great Salt Lake. Viveiros' (1986) basin model shows an asymmetric basin geometry with a shallow eastward dip of approximately 12° to 15° from Stansbury and Carrington islands to the deepest (> 3.0 km) part of the basin. The east side of the basin is bounded by a west dipping listric normal fault with about 3 to 4 km of offset. Radkins (1990) developed and used a three-dimensional gravity inversion routine to generate a basin model of the Salt Lake Valley. Radkins' (1990) basin model shows a broad relatively shallow (< 0.3 km) basin geometry with two deeper, but still quite shallow (< 1.1 km) areas, one of which is located northwest of Salt Lake City and the other in the east-central part of the model near Sandy, Utah.

Geologic Setting

One manifestation of the complexity of this area is the geology. Rocks of the Farmington Canyon complex, of Archean to Early Proterozoic age (>1600 m.y.), are exposed on Antelope and Fremont islands, from Bountiful to Ogden east of the Wasatch fault, and on Little Mountain west of Ogden (Figure 2). The dominant rock types in the Farmington Canyon complex are granitic gneiss, migmatite, gneiss and schist (Bryant, 1984). Paleozoic rocks are exposed at the northern end of Antelope Island, in the Oquirrh and Promontory mountains, and east of the Wasatch fault from Ogden to the northern end of the study area (Figure 2). The major Paleozoic rock types in the study
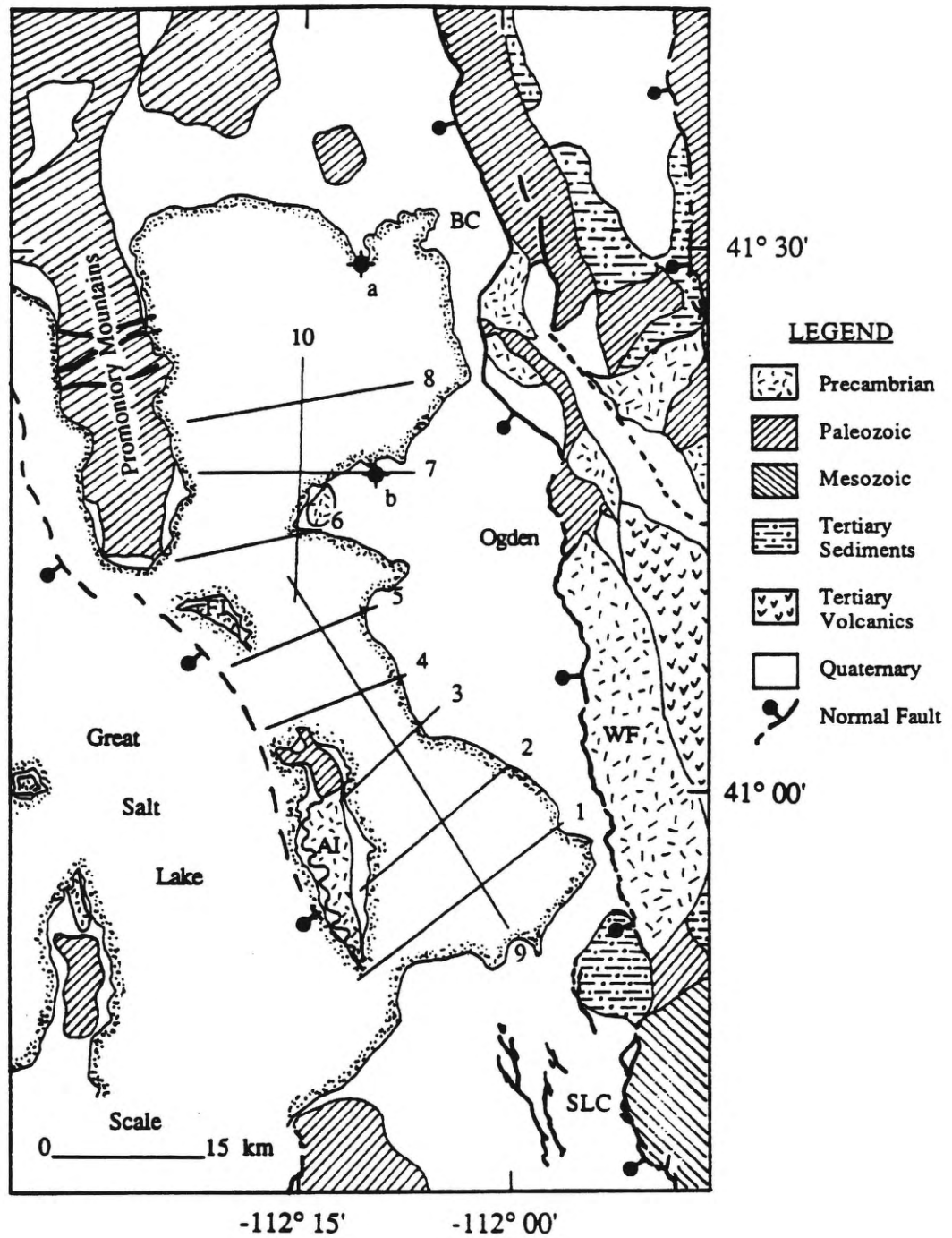
Figure 2. Map showing the general geology of the study area from Hintze (1980). Location of normal faults on the Promontory Mountains from Olson (1960). WF = Wasatch fault, SLC = Salt Lake City, BC = Brigham City.

area are quartzite, limestone and dolostone. No rocks of Mesozoic age are exposed in the study area, but they are present south of the Salt Lake salient. Tertiary age rocks of the Wasatch Formation are exposed at the Salt Lake salient and Tertiary age volcanics are exposed east of the Farmington Canyon complex from Bountiful to Ogden. The center of the study area is covered by Quaternary sediments. These sediments are predominantly Bonneville Lake sediments, mud and salt flats. There are large gaps in the stratigraphic sequence between the >1600 m.y. old Farmington Canyon complex and Paleozoic rocks and between the Paleozoic and Cenozoic rocks. These gaps indicate a depositional hiatus associated with tectonic activity, such as uplift and associated erosion and faulting.

Regional Tectonics

The geologic complexity of the study area is a result of tectonic activity during the past 100 m.y (Yonkee, 1990). This area has been subjected to compressional followed by extensional tectonic forces over this time period.

Compressional Tectonics

Two major compressional tectonic events have left their signature on the structural complexity of the study area. The Sevier Orogeny, which was active from approximately 105 to 70 m.y.b.p. (Stokes, 1986), produced a series of thrust sheets in central and northern Utah that get younger from west to east (Hintze, 1988) and is part of the Idaho-Utah-Wyoming Overthrust belt. Hintze (1988) shows that there are five separate thrust systems in northeastern Utah. The Absaroka ramp-anticline which trends north-south from Bountiful to Ogden 10 km east of the Wasatch fault (Figure 3) is thought to have been formed at this time (Yonkee, 1990). The complex structural geometries produced by these thrust sheets and their geographic orientations are shown
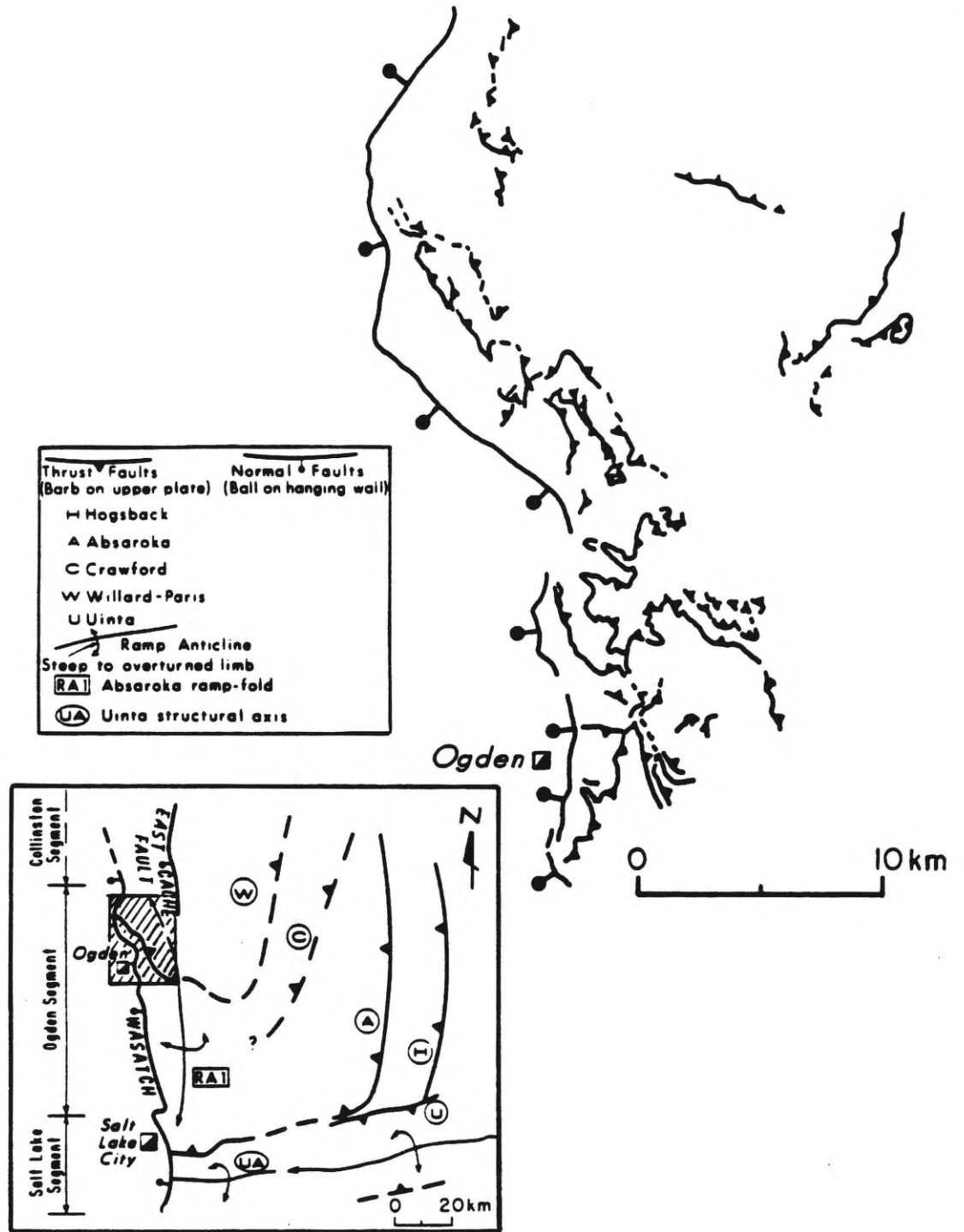
Figure 3. Map showing the general (bottom) and detailed (top) compressional structures in the study area. General structures from Smith and Bruhn (1984) and detailed structures from Davis (1985).

in Figure 3. The Laramide Orogeny, assumed to be active from approximately 80 to 40 m.y.b.p., is thought to be responsible for the formation of the Uinta Mountains and associated structures which extend in all directions (Stokes, 1986). Some of these associated structures, such as the Salt Lake salient, extend to and possibly through the Wasatch Front.

Extensional Tectonics

The formation of the Basin and Range province over the last 15 to 20 m.y. (Hintze, 1988) is the primary extensional tectonic event in this region. The major component of the extension direction is east-west. In the most simplified models the Basin and Range province is represented as a series of ranges and asymmetric basins trending north-south and extending from the eastern front of the Sierra Mountains to the Wasatch Front.

ACQUISITION OF DATA

Three types of data were used in this study: 1) industry seismic reflection profiles; 2) complete Bouguer anomaly gravity data; and 3) well data (geophysical logs showing depth to basement). These geophysical data sets provide the most complete geophysical information available for the study area and the combination of these data produces optimal resolution and spatial coverage of the Weber Basin.

Seismic Reflection Data

The criteria used for selecting the seismic profiles in this study were the quality of data and the extent of data processing. Data quality is highly dependent on the fold number (number of times each common depth point is sampled) and the source type (explosive or vibrator) of the seismic data. Data of at least 24-fold with an explosive source were preferred. Wave equation migration and associated processing (secondary statics corrections, secondary velocity analysis and predictive or spiking deconvolution) was a minimum requirement for processing. Ten seismic reflection profiles meeting these requirements were acquired by Elf Aquitaine Petroleum (EAP) between 1979 and 1980. EAP shot these 24-fold data using a 200 grain Primacord explosive source. The locations of the profiles used are shown in Figure 1. These data were processed by EAP with the general background information listed in Table 1.

Additional seismic profiles from CGG and Celcius Energy were examined, but were not used in this study. I had little confidence in the basement picks from these data because of poor data quality. The seismic profiles acquired at Hill Air Force Base by Seismograph Service Corporation under contract to the University of Utah Research Institute were not used for the same reasons.

Table 1

General information for seismic reflection profiles used in this study.

Profile	Source	Datum (ft)	Station Spacing(ft)	Fold	Migration
Line 1	Primacord	4193	165	24	Wave Eq.
Line 2	Primacord	4193	165	24	Wave Eq.
Line 3	Primacord	4193	165	24	Wave Eq.
Line 4	Primacord	4193	165	24	Wave Eq.
Line 5	Primacord	4193	165	24	Wave Eq.
Line 6	Primacord	4193	165	24	Wave Eq.
Line 7	Primacord	4193	165	24	Wave Eq.
Line 8	Primacord	4193	165	24	Wave Eq.
Line 9	Primacord	4193	165	24	Wave Eq.
Line 10	Primacord	4193	165	24	Wave Eq.
Line R11	Primacord	4200	220	12	Time

Gravity Data

A subset of the complete Bouguer anomaly gravity data for Utah compiled by Cook et al. (1989) was used in this study. These data are the most recent and complete available for Utah. Latitude and longitude, elevation and terrain corrections were applied to the observed gravity data using the 1967 gravity formula (Cook et al., 1989) to produce the complete Bouguer anomaly data. This subset consists of approximately 1700 gravity measurements which were used to produce a residual gravity map of the study area. The distribution of these measurements is shown in Figure 4 and the complete Bouguer anomaly gravity map for the area is shown in Figure 5.
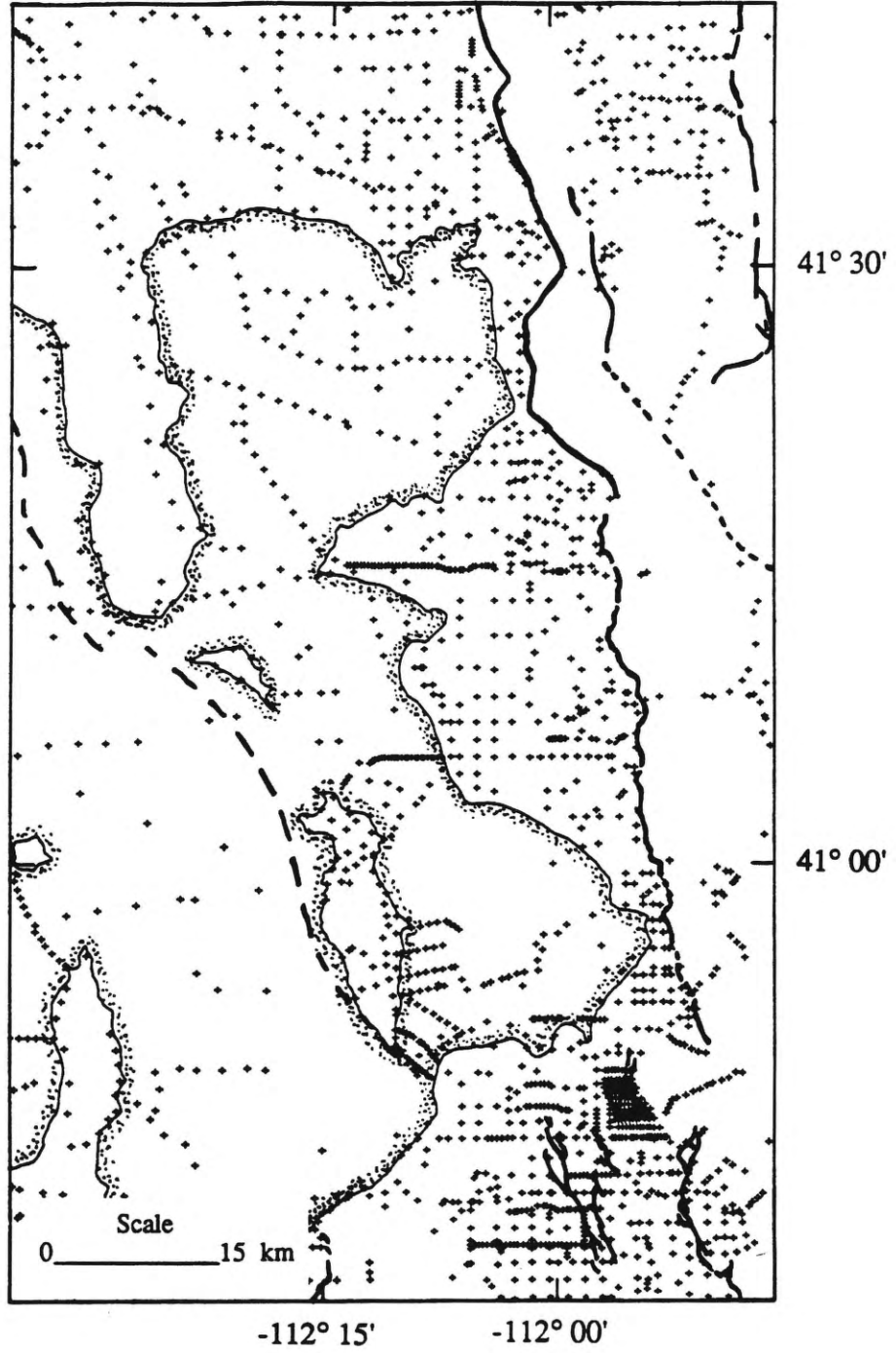
Figure 4. Plot showing the distribution of gravity measurements in the study area. Locations are marked by "+".
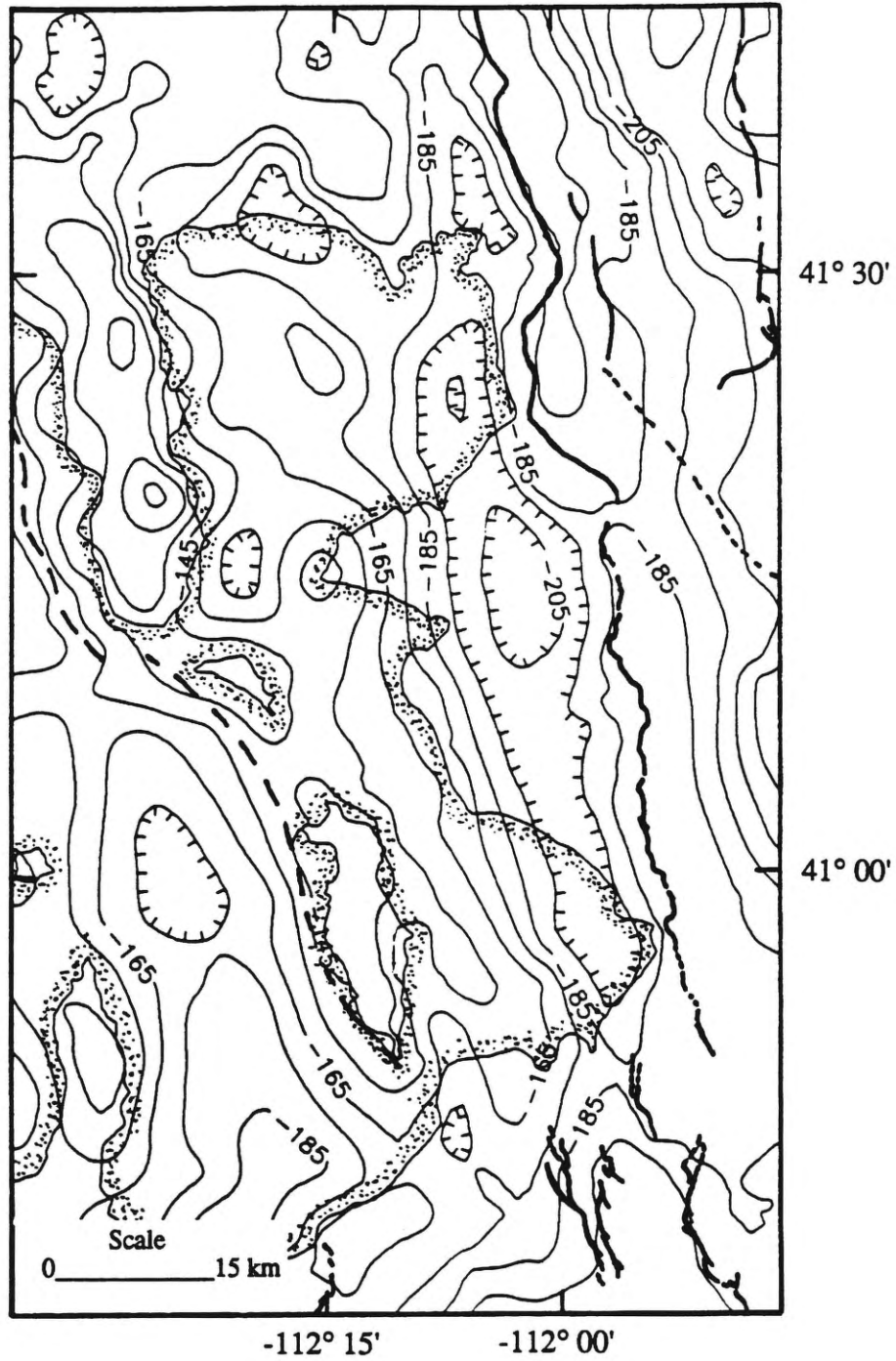
Figure 5. Complete Bouguer anomaly gravity map for the study area. Contour interval 10 mGal.

Well Data

Well log data were obtained from the Utah Oil and Gas Commission. The criteria used in selecting the well data were proximity to seismic profiles, the types of well logs available for each well, and well depth. Wells had to be close enough to the seismic reflection profiles to correlate seismic reflectors to geophysical data from the well logs. Acoustic velocity and density logs were a minimum requirement for the geophysical logs. Wells that penetrated basement were preferable, but wells over 1000 meters deep with geophysical logs were acceptable. Well logs from two wells, of 15 examined, met these criteria and were used in this study (Table 2). Well "a" penetrated bedrock, interpreted to be of Paleozoic age, at a depth of 1070 m.

Table 2

General information on wells used in this study.

	Company	Name	Total Depth Drilled(ft)	Interval Logged(ft)	Type of Log
Well "a"	Burnett Oil Co.	D. Christensen # 1–9	6000	1010–5985	Density Velocity
Well "b"	Burnett Oil Co.	Basin Investment #1	4817	978–4816	Density Velocity

THEORY

In this study the gravity data were inverted for the basin geometry using a damped and weighted least squares algorithm. A brief discussion of the theory behind the method developed by Richardson and MacInnes (1989) is given below.

Inversion Theory

The weighted and damped least squares inversion method is a modification of the ordinary least squares method (Menke, 1984). The ordinary least squares and associated methods solve a system of linear equations which can be expressed as,

$$\mathbf{d} = \mathbf{Gm},$$

where $\mathbf{d}$ is the observed data vector, $\mathbf{G}$ is the sensitivity matrix and $\mathbf{m}$ is the model parameter vector. For the nonlinear problem $\mathbf{m}$ is expanded in a Taylor's series about $\mathbf{m}_k$, the estimate of model parameter vector after the kth iteration. The linearized model parameter update is written as

$$\mathbf{m}_{k+1} = \mathbf{m}_k + \Delta \mathbf{m}.$$

Weighted Least Squares

Under some circumstances it is useful to use weighted measures of the prediction errors (Menke, 1984). Usually, some observations or measurements are made more accurately than others. A way of taking this into consideration in the inversion method is to weight the effects of each measurement by its predicted error. For our purposes this weighting factor is the inverse of the covariance matrix of data errors C_d^{-1}. A generalized prediction error E_d is defined as

$$E_d = e_d^T C_d^{-1} e_d,$$

where $e_d = (d - Gm)$.

A weighting matrix C_m^{-1} can also be applied to errors associated with the model parameters. C_m^{-1} is the inverse of the covariance matrix of errors with respect to the starting model m_o. A similar generalized prediction error E_m is defined as

$$E_m = e_m^T C_m^{-1} e_m,$$

where $e_m = (m - m_o)$.

Fitting noisy data and staying close to a starting model can be conflicting goals (Richardson and MacInnes, 1989). A reasonable way of dealing with this conflict is to take a weighted sum of the two criteria,

$$E_t = E_d + \gamma E_m,$$

where the choice of $\gamma > 0$ determines the trade-off between fitting the data and staying close to the starting model.

Applying a least squares minimization to E_t,

$$\nabla E_t = 0,$$

where ∇ is the gradient operator and substituting the appropriate variables we get

$$m_{k+1} = m_k + [G^T C_d^{-1} G + \gamma C_m^{-1} + \lambda D]^{-1}[G^T C_d^{-1} \Delta d + \gamma C_m^{-1}(m_o - m_k)],$$

where $\Delta d = (d_{obs} - d_{pred})$ with d_{obs} being the observed data vector and d_{pred} the predicted data vector, λ is the damping factor, and D is a diagonal matrix composed of the diagonal elements of $G^T C_d^{-1} G$ (Richardson and MacInnes, 1989).

The advantage of a weighted damped least squares algorithm is that the user can penalize solutions that deviate from the desired one. A situation where this is very useful is when geologic or other geophysical information is available to constrain the initial model.

The computer program written by Richardson and MacInnes (1989) was modified to run on a Sun 4/390 computer and then was tested using two test data sets

included with the program. The results from running these data sets were identical to the results of Richardson and MacInnes (1989).

ANALYSES OF DATA

Seismic Data Analysis

Identifying the location of the Tertiary age basin fill and acoustic basement contact on each seismic profile involves geophysical interpretation and geologic insight. The geophysical background used for interpreting the contact included knowledge of seismic stratigraphy (identifying onlap, offlap, etc.), basic reflection seismology principles (understanding of impedance contrasts, etc.), signal analysis and seismic processing methods (separating seismic energy associated with actual impedance contrasts from that which is not) and scientific intuition. Using this background knowledge, the location of the acoustic basement contact was estimated. The interpreted basement reflectors are labelled in Plates 1–6.

At each shot point or common depth point where normal moveout and interval velocities were calculated for stacking the seismic data, the depth to basement was calculated. The depths were then used to produce depth-to-acoustic-basement profiles along the seismic lines (Figures 6 and 7). These profiles show the gross geometry of the west side of the basin, which varies more in the east-west direction than in the north-south direction.

The basement depths from each profile were combined with known coordinates of the basin edge, the surface trace of the Wasatch fault and along the shoreline of Antelope and Fremont islands and the Promontory Peninsula, to produce a depth-to-basement contour map (Figure 8). The depth values were gridded using MINC.F, which is a minimum curvature gridding routine (courtesy of R. Simpson, U. S. Geological Survey) and then contoured using a program in the Surfer Software package (Trademark of Golden Software Company, Golden, Colorado). The minimum
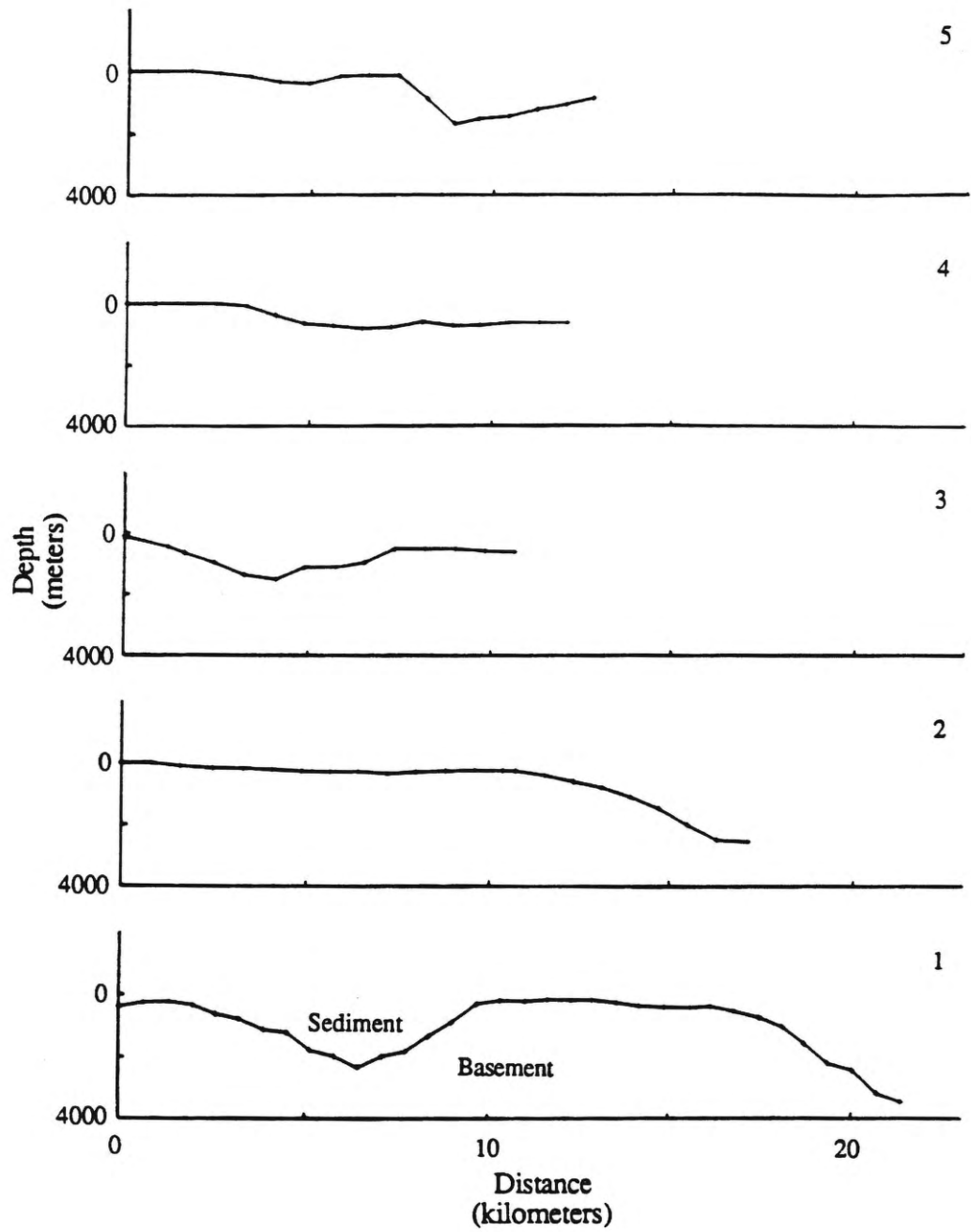
Figure 6. Depth-to-basement profiles for seismic reflection lines 1–5.
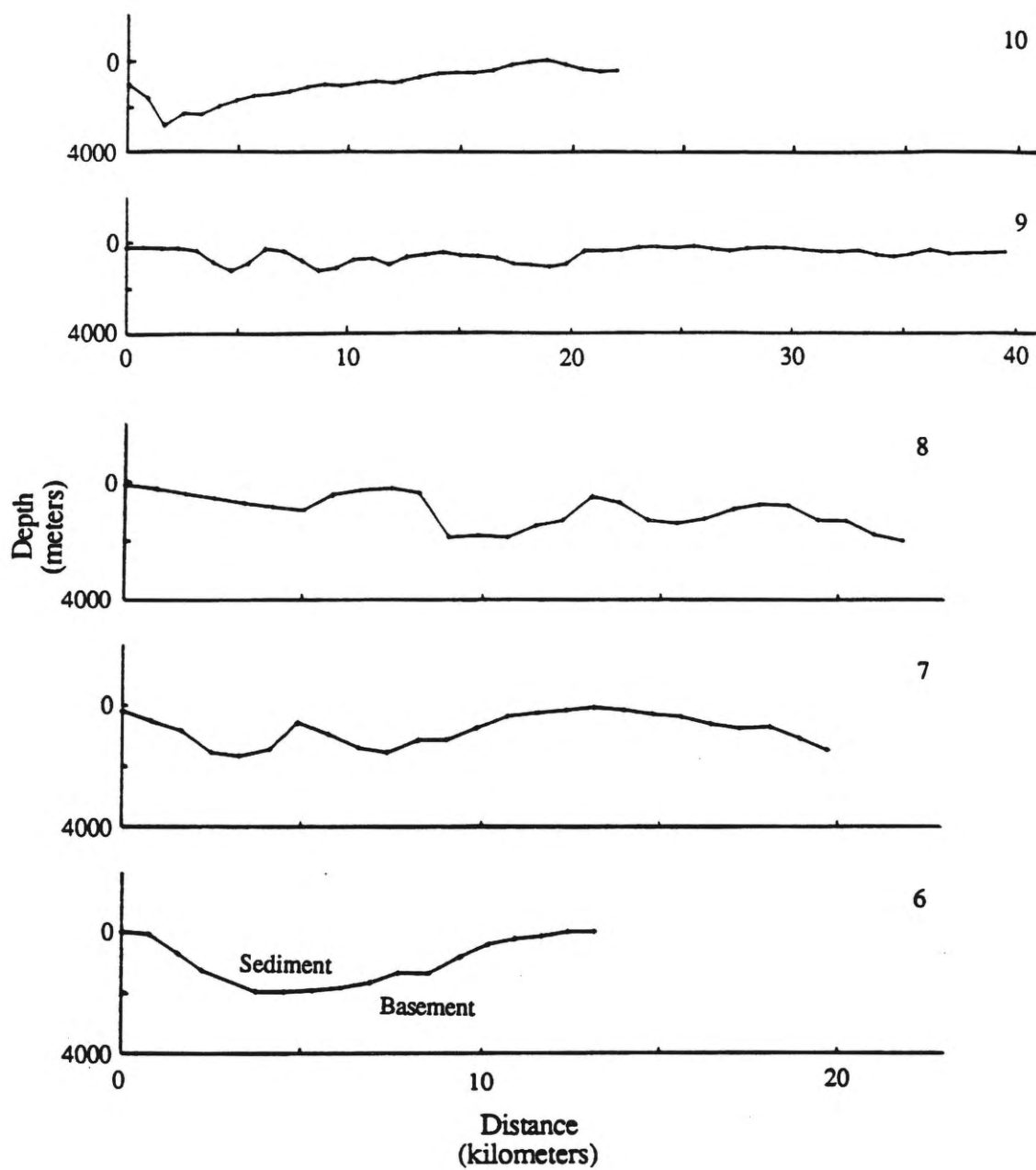
Figure 7. Depth-to-basement profiles for seismic reflection lines 6–10.
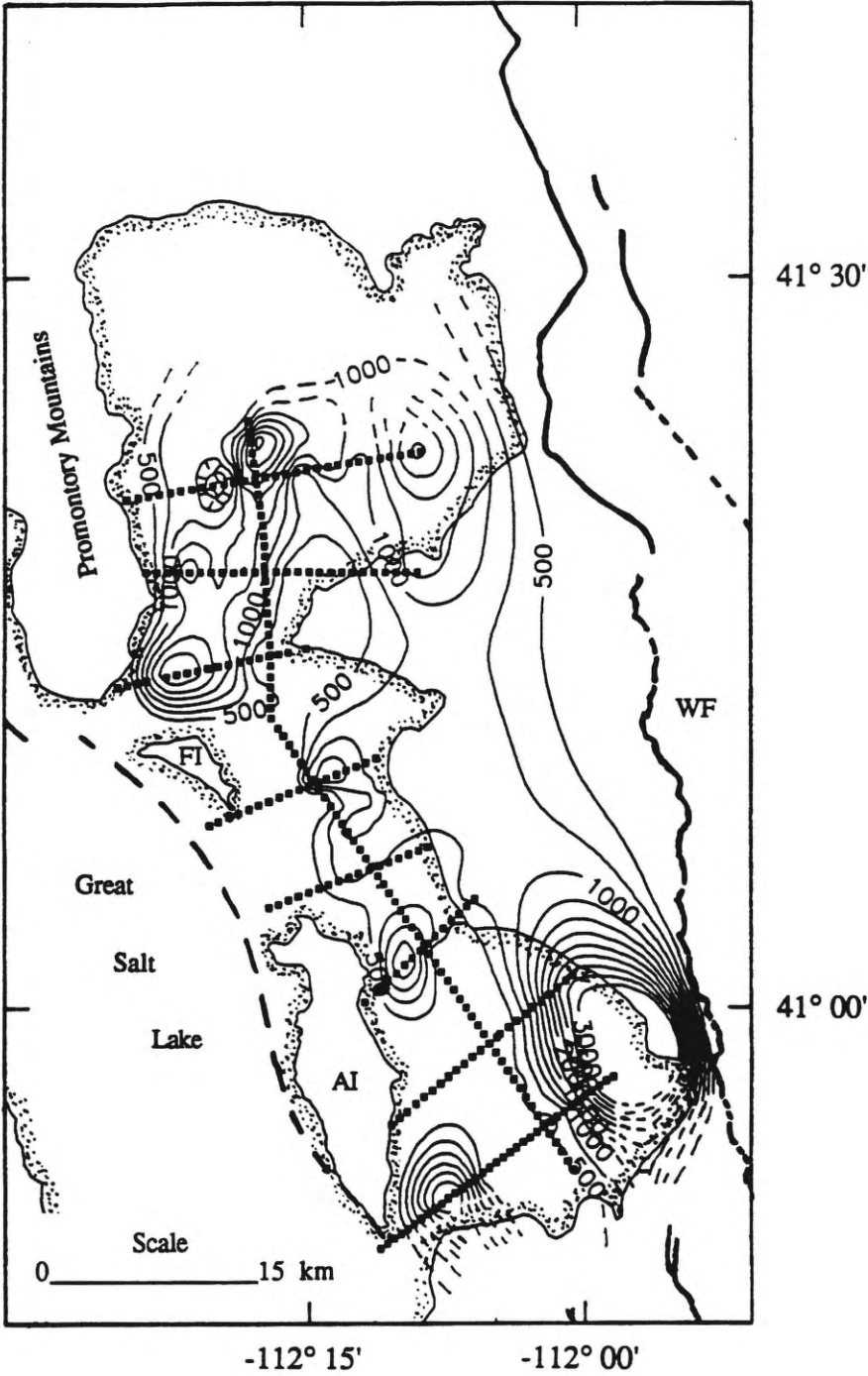
Figure 8. Depth-to-Basement contour map of the study area from the seismic reflection profiles. Contour interval is 500 m; squares show locations of depth values calculated from the seismic data. Hachures indicate closed basement highs.

curvature algorithm has no radius of influence constraint and therefore grids the whole data set with equal weight. In areas with no depth information the contours were dashed by hand.

Well Data Analysis

The rationale behind the well log analysis was to see if the impedance contrasts recorded in the logs correlated with reflectors in the seismic reflection profile, and if so, how good is the correlation?

The location of the two wells used in this study are shown in Figure 1. Acoustic velocity and density profiles were produced from the acoustic velocity and density logs for these wells (Figure 9). The profiles were produced by identifying differences in density of greater than 0.1 g/cc and acoustic velocity differences greater than 0.25 km/s consistent over an interval of 30 m, which is the approximate spatial resolution of the seismic reflection data.

An impedance model was generated from the acoustic and density profiles. From this impedance model a zero offset synthetic seismogram was generated using the reflectivity method (Fuchs and Muller, 1971) and compared to the corresponding section from Line 7 (Figure 10).

The correlation between the synthetic seismogram and the seismic reflection profile is very good as can be seen in Figure 10. The acoustic velocity and density contrasts shown in the well logs produced synthetic reflections at two-way traveltimes comparable to the actual seismic reflection profile. The strong doublet reflection located at about 400 msec and the reflection located at about 1000 msec match the reflections in the seismic reflection profile at these times very closely in amplitude, phase and frequency. It is unreasonable to expect a one-to-one correspondence between the synthetic reflections and the real data reflections because the well log profiles are smoothed representations of the actual rock properties recorded in the well logs. This
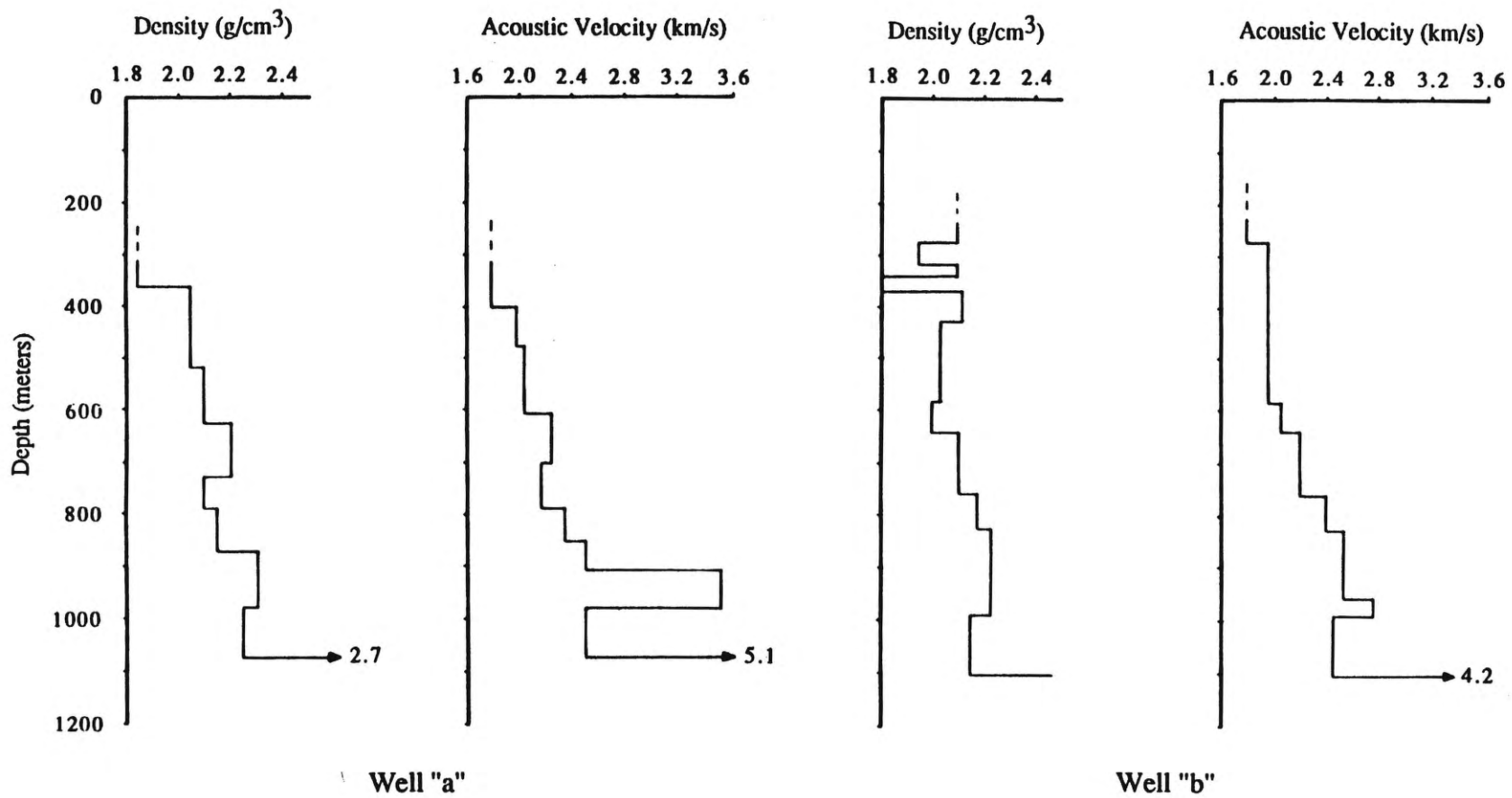
Figure 9. Acoustic velocity and density profiles for wells "a" and "b".
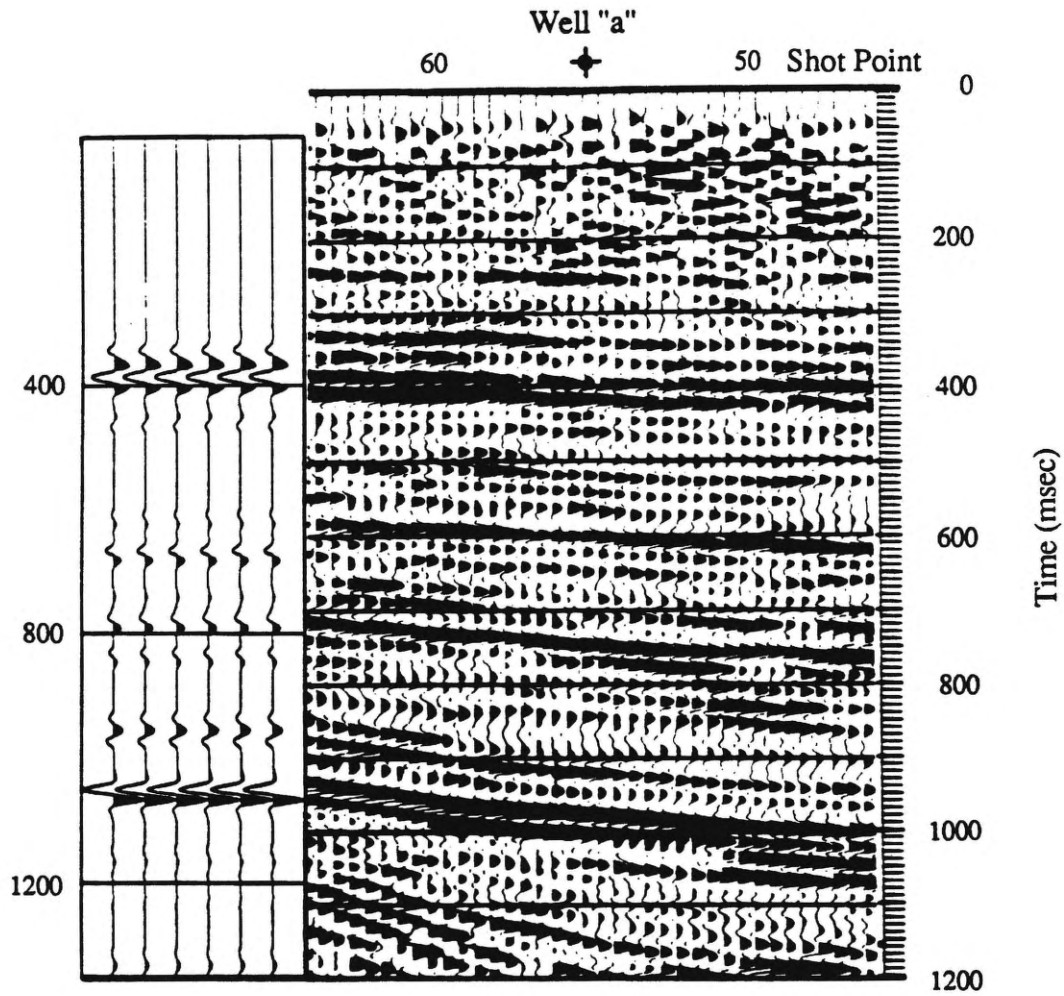
Figure 10. Comparison of synthetic seismogram and corresponding section of Line 10. Location of Well "a" and shot points are labelled on top of figure.

analysis lends confidence to the depth to basement calculations from the seismic reflection profiles because the depth of the large impedance contrasts in the logs correlated with the calculated depths from the seismic profiles.

The density-depth profiles produced in this study were used to calculate a weighted average density contrast between the basin sediments and basement rock, as described by Litinsky (1989). The weighted average was calculated by summing all the products of the density contrasts of each discrete layer with respect to the basement and the thickness of each layer, then dividing this sum by the depth of the basin. This calculation resulted in an average density contrast of -0.53 g/cc and was used in the three-dimensional gravity inversion.

Gravity Analysis

The gravity data were used to determine the basin geometry in locations where other geophysical and geologic data were not available. The analysis of the gravity data involves estimating the gravitational effects of deep crustal and upper mantle compensatory features and subtracting these effects from the data to enhance the shallower features. These residual gravity data were then used to determine the basin geometry.

The gravity data were sorted by latitude, longitude and elevation to include only those points in the study area. A subset consisting of 1098 gravity measurements was separated from the approximately 1700 measurements in the Weber basin vicinity to be used in the inversion of the gravity data. The locations of these 1098 measurement were plotted and compared to the seismic line locations. Combining the two data sets yields very good coverage of the area (Figure 11).
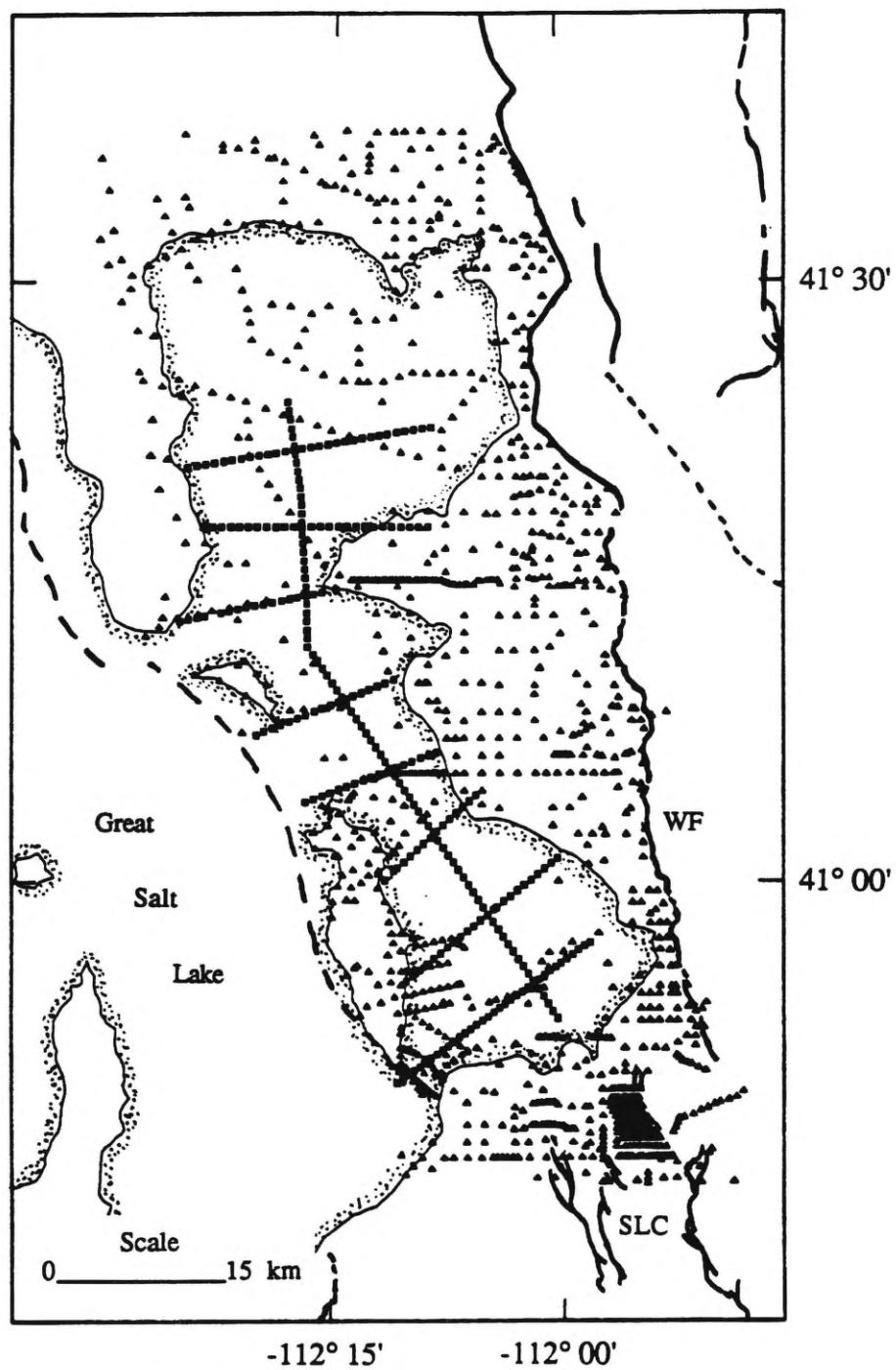
Figure 11. Distribution of seismic reflection and gravity data over the study area. Note the very good coverage. Squares represent seismic data locations; triangles represent gravity data locations.

Regional Gravity Field

It is intuitively obvious gravity measurements contain geophysical information pertaining to the measurement location, but how one separates the wanted information from the unwanted information is a method wrought with personal biases. My personal biases are toward using models generated from estimates of the earth's physical properties as opposed to mathematical curve-fitting models to calculate regional effects and using the original data points rather than gridded data for input into inversion programs.

The regional gravity model employed for this study considers an isostatic compensation depth and an elastic plate thickness to calculate the large scale regional effects of isostatic compensation of surface topography and upper crustal loads. The algorithm, written by Tony Lowry, was generated from equations for flexure of the lithosphere due to periodic loading discussed in Turcotte and Schubert (p. 122–123 and p. 221–222, 1982) as well as an upper-crustal load deconvolution developed by Cordell, Zorin and Keller (1991). The estimates of physical parameters used to calculate the regional gravity field are: an elastic plate thickness of 8000 m; a continental crust density of 2670 kg/m^3; an upper mantle density of 3200 kg/m^3; a depth of compensation of 25000 m; a Poisson's ratio value of 0.25; and a Young's modulus value of 10^{11}.

The residual complete Bouguer anomaly gravity map from this model is very similar to the isostatic map produced by Simpson, Jachens, Blakely and Saltus (1986) for the continental U.S., with less than approximately 10% variation of the amplitude and wavelength of the gravity fields between the two maps. This similarity is comforting because the algorithms for calculating the two regionals are not the same.

Unfortunately, this regional removal process did not completely isolate the gravity effects of the basin because effects caused by loading at the base of the crust cannot be predicted. Basin analysis using gravity data requires modeling negative

density contrasts unless one is dealing with the rare case of the basin sediments being more dense than the basement rocks. The isostatic residual generated here had a positive aspect over portions of the Weber Basin. To overcome this final difficulty, a best fit planar surface was calculated using gravity values from the edge of the basin at or near bedrock and then subtracted from the gravity values located in the basin. This guaranteed the negative density contrast between the basin sediments and bedrock needed for the gravity inversion as can be seen in Figure 12.

Gravity Modeling

Barnett (1976) developed the three-dimensional forward model used in the inversion routine. The basin is modeled as a polyhedron made up of triangular facets which can be any size and have as many facets as needed to define the body, up to the parameter limits of the inversion program. For this study, the x and y position of the facet is fixed and its depth is allowed to vary for the points being inverted. The computer program, as written, limits the number of unknown depth nodes to 50 and the total number of depth nodes for the model to 102. This limit was restrictive, but was overcome by using two models to cover the extent (35x90 km) of the study area. Model 1 covers the lower two-thirds of the study area; model 2 covers the upper one-third. The models overlap by one row of inversion nodes.

Model 1 encompasses the area of the seismic data used in this study. The depth to basement on the west side of the model was fixed using the depths calculated from the seismic reflection profiles. Model nodes east of the surface trace of the Wasatch fault were fixed at zero depth. The inversion nodes were positioned to maximize the coverage over the areas where seismic data was sparse or nonexistent. The approximate spacing between these nodes is 4 to 5 km in both the x and y directions. The spatial
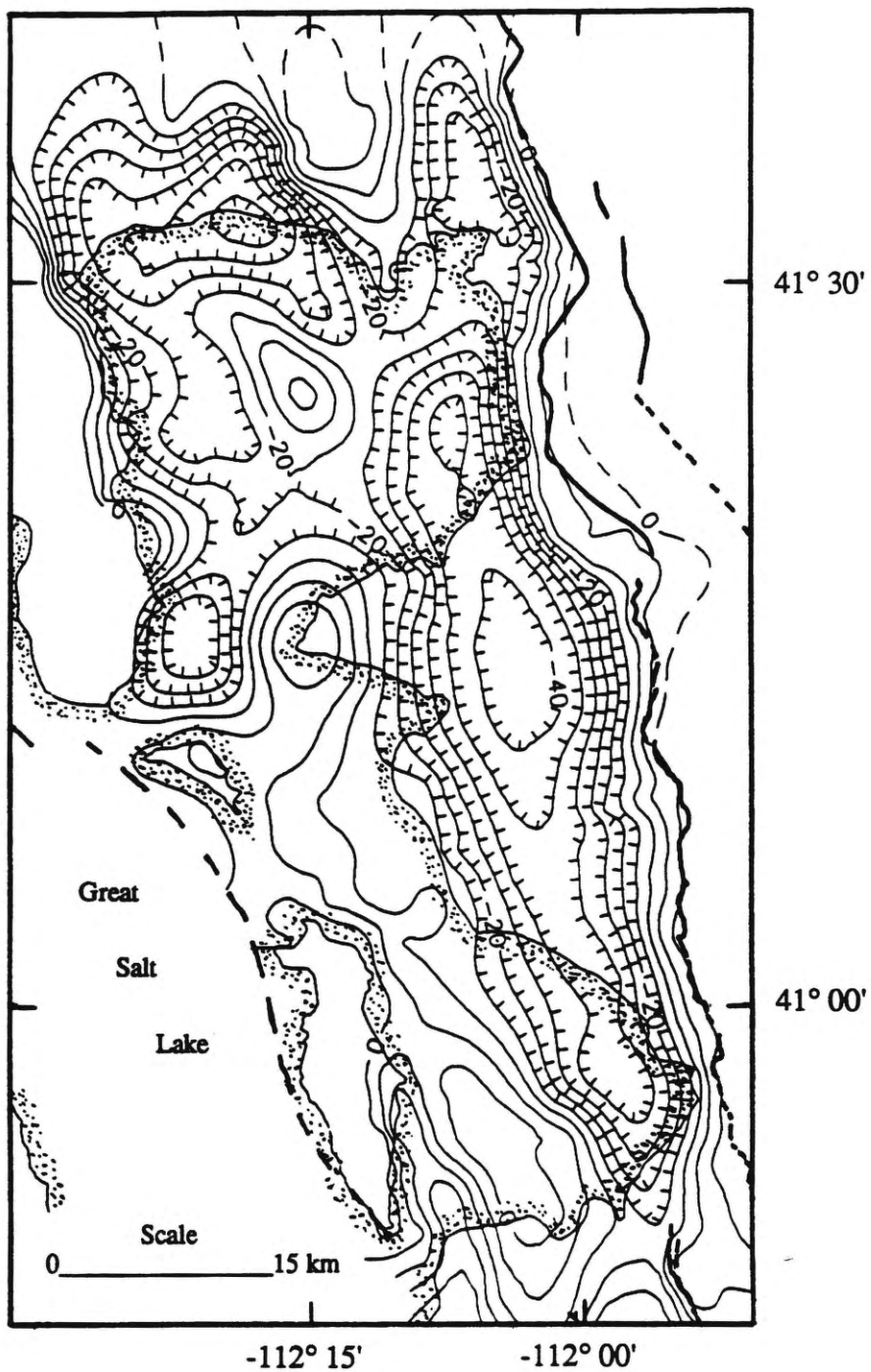
Figure 12. Contour map of residual gravity data used in the gravity inversion routine. Contour interval is 5 mGal.

41° 30'

41° 00'

-112° 15'   -112° 00'

Great

Salt

Lake

Scale

0_____15 km

resolution of this model is adequate based on the geometry of the study area and the distribution of gravity station measurements.

Model 2 was generated with the same x-y node spacing as Model 1, but had no seismic depth constraints. Node points located on the edge of the basin and east of the Wasatch fault were fixed at zero depth. The initial depths for the node points were set at zero. Due to the lack of depth control over the model area this is effectively an unconstrained gravity inversion.

Both initial models were fed to the inversion routine using a density contrast of -0.53 g/cc, an initial ridge regression (Marquardt) damping factor, λ, of 1.0 and a maximum number of 10 iterations. The model-parameter-versus-observed-gravity weighting factor, γ, was set to 1.0 for Model 1. A value of 1.0 gives equal weight to the model parameters and observed gravity values. This value was used because the model is well constrained. This is not the case for Model 2 so the weighting factor was set to 0.5. This value weights the observed gravity data more heavily than the initial model parameters and thus favors a solution honoring the observed gravity data.

A depth-to-basement contour map was produced by combining the calculated depths from the seismic reflection profiles and the gravity inversion results (Figure 13). The latitude, longitude and depths for this basin model are listed in Appendix A. As can be seen by comparing Figures 8 and 13, the Figure 13 contour map has considerably more resolution. The basin geometry of the area east of the seismic profiles and west of the Wasatch fault is well defined in Figure 13.

Minor editing was done to the results of Model 1. For example, the two node points which had depth values above the valley surface, both < 0.27 km, were set to zero depth. These points are located at the edge of the valley along the Wasatch fault, which is at the edge of the density contrast and could explain their deviant behavior. Otherwise, all the calculated depths produced by the inversion program were used.
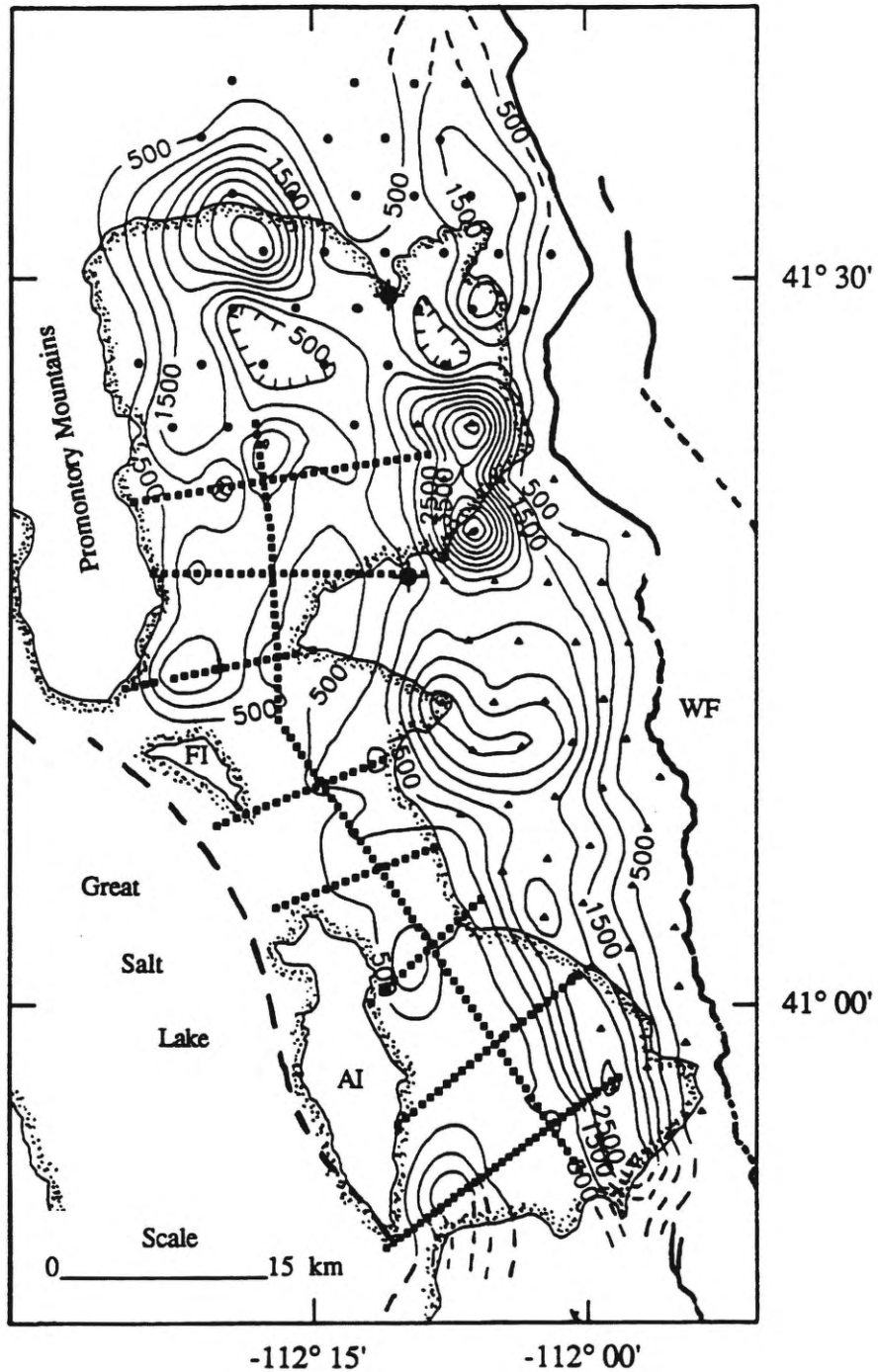
Figure 13. Depth-to-basement contour map from seismic reflection data (squares) and results of the inversion of gravity data. Triangles represent depth points determined from Model 1 and dots represent depth points determined from Model 2. Contour interval is 500 m. Hachures indicate closed basement highs.

Due to the lack of depth constraints for Model 2 a different approach was used in editing the results. The errors between the calculated and observed gravity values used in the inversion were contoured, and the depths associated with Model 2 were also contoured. Node points located in regions with errors greater than 2 mGals were removed; 15 points were deleted.

The basin model produced in this study shows an anomalous depression west of the Wasatch fault between North Ogden and Brigham City. The northern edge of this depression is located at the seam between Model 1 and Model 2. A second set of models were produced to test the effects of the seam on the basin model (Figure 14). Model 1 was extended approximately 8 km northward to minimize edge effects over the depression. As one can see by comparing Figure 13 with Figure 14 there are no significant differences between the basin models.
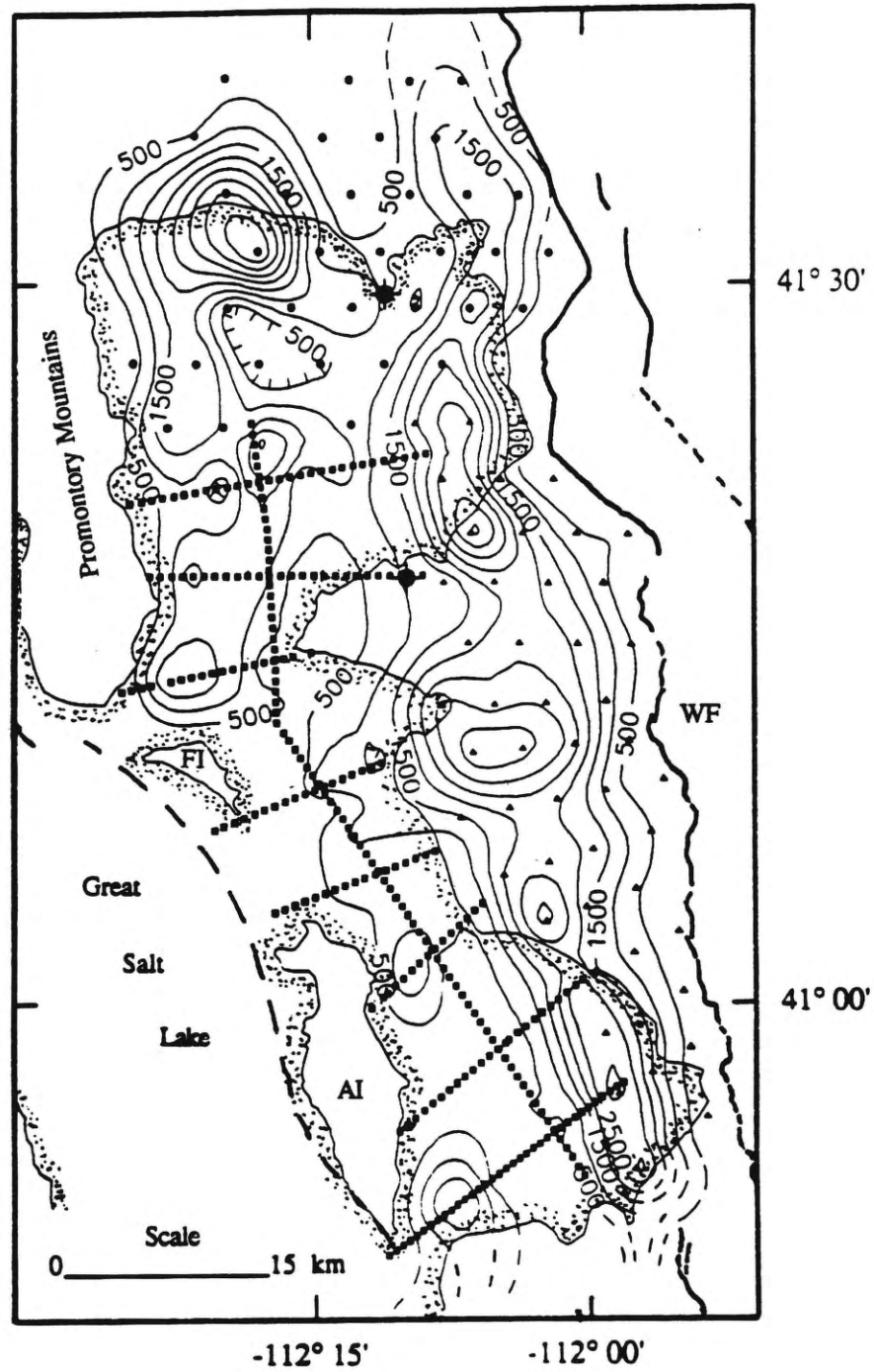
Figure 14. Depth-to-basement contour map with seam between Model 1 and Model 2
shifted about 8 km north. Contour interval is 500 m. Hachures indicate
closed basement highs.

INTERPRETATION

Seismic Interpretation

Seismic profiles 1, 2, 3, 6, 7, and 8 (Plates 1–5) show similar basin geometries and structural features associated with two local basins, one east of Antelope Island and the other east of the Promontory Peninsula. These six profiles show east dipping Tertiary sedimentary sequences downlapping on to the Precambrian and Paleozoic basement. The sedimentary sequences show toplap into a possibly late Tertiary or Quaternary age unconformity. The clearest example of this geometry is shown in Line 6. The direction of downlap infers that the sediment transport direction in these basins was west to east. The center of profiles 1, 2, 7, and 8, and the east side of profiles 3 and 6 show the basement high which trends north-south over the length of the study area.

The west side of seismic profiles 4 and 5 (Plates 2 and 3) show the shallow sediment-basement reflector between Antelope and Fremont islands. The center and east side of these profiles show Tertiary sediments gently dipping into the main basin. As with the other profiles, the inferred sediment transport direction from these profiles is west to east.

All of Line 9 and the southern half of Line 10 (Plates 5 and 6) elucidate the geometry of the basement high which is covered by thin (< 750 m) Tertiary and Quaternary sediments. The northern half of Line 10 shows the sediment-basement contact dipping north into a local basin. The north end of Line 10 shows evidence of a normal fault with an apparent dip of 38° to the south. The gently folded Tertiary sediments are truncated above by an unconformity and to the north by this normal fault. The normal fault does not appear to penetrate the unconformity.

Olson (1960) mapped a series of normal faults in the Promontory Mountains, three of which (Figure 2) trend toward the normal fault shown on the north end of Line 10. One of these three faults, the Chokecherry fault, shows the same sense of displacement (north side up-south side down) as the Line 10 fault. A dip angle for the Chokecherry fault is not given, so a comparison of the two faults is not possible.

If one assumes the Line 10 fault trends sub-perpendicular (east-west) to Line 10 and projects eastward to the Wasatch fault it presents a new interpretation of the Weber Basin geometry in this area. In the basin model the north side of the depression between North Ogden and Brigham City west of the Wasatch fault has a dip of about 37° south which is 1° less than the calculated apparent dip of the Line 10 fault. Also, the Brigham City fault segment is thought by some investigators (Bruhn, personal communication, 1991) to end where the Line 10 fault projects into the Wasatch fault. If the Line 10 fault does project eastward across the Weber Basin its presence can help explain the complex geometry in this area.

At the south end of the basin one continuous coherent reflector (R2), which I interpret to be the sediment-basement contact, is present on Line R 11 (Plate 6). As one can see by comparing Line R 11 with the other ten seismic profiles, interpretation of Line R 11 is considerably more difficult.

Yonkee (1990) produced a balanced geologic cross-section from the northeast of Antelope Island eastward to the Wasatch Mountains on the basis of extensive geologic mapping and modeling. He shows a west dipping thrust fault east of Antelope Island which is part of the Ogden Thrust System (Yonkee,1990). Though the fault is not exposed at the surface and the actual location is unknown, its presence is necessary to meet balancing constraints. Seismic profiles 2 and 3 (Plates 1 and 2) show what I interpret to be this fault, although its location is farther west than shown in the cross-

section. This was the only interpretable feature in the Paleozoic or Precambrian sections.

The east side of seismic profiles 1 and 2 (Plate 1) show evidence of en echelon down stepping normal faults from the Wasatch Front westward into the basin. A similar geometry is observed on a smaller scale by Stephenson (1991). These faults propagate through various levels of Tertiary age reflectors. During the formation of the basin, stress may have been released on various faults at various times rather than activating the most basinward fault on the range front. If this is the case displacement could occur on one or more of these faults due to an earthquake.

An antithetic normal fault is also interpreted to be located on the west slope of the basin forming a graben structure at the basin bottom. This interpretation is similar to that of Wilson et al. (1986) for seismic Line 1. The steep dipping normal fault shown in Yonkee's (1990) cross-section is not observed in the seismic profiles. This is not surprising considering steep dipping normal faults are not readily imaged by standard reflection seismology techniques.

Well Log Interpretation

A major question related to this section is: can the R2 reflector discussed in Arnow and Mattick (1968), defined by Hill (1988) and used by Radkins (1990), be correlated to reflectors in the Weber Basin? The answer is yes, but not as defined by Hill (1988). My interpretation differs from Hill's (1988) as to what the R2 reflector represents. Hill (1988) classifies the R2 reflector as being the contact between semi-consolidated and consolidated Tertiary sediments. The discussion in Arnow and Mattick (1968) and geophysical logs from nearby wells do not agree with this interpretation. A more consistent interpretation is that the R2 reflector represents the sediment-basement contact. Using this definition the two reflectors are compatible.

Velocity and density logs from seven wells in the west side of the Great Salt Lake were examined. Depths to the top of the Pliocene, Miocene and Paleozoic or Precambrian deposits are listed by Viveiros (1986). For all seven wells the top of the Pliocene and Miocene deposits are not associated with a distinct impedance contrast. Some other criteria must have been used to determine these boundaries. The only boundaries showing distinct impedance contrasts are the Pliocene or Miocene-Paleozoic or Precambrian contacts.

Assuming this same condition applies to the basin on the east side of the lake, the prominent reflectors seen in the seismic profiles are not associated with the Pliocene or Miocene boundaries, but are associated with impedance contrasts in these sequences. Consequently, no prominent reflector can be directly correlated with these boundaries. The one boundary which can be defined by a prominent reflector is the Tertiary-Paleozoic or Precambrian contact. Determining the depth to this boundary is the objective of the 3-D gravity inversion.

Gravity Interpretation

Zoback (1983) used a regional complete Bouguer anomaly gravity map to interpret basement structures which possibly affected Cenozoic basin formation and normal faulting. A similar regional interpretation is discussed here, but the interpretations are made from a residual complete Bouguer anomaly gravity map. Distribution of gravity measurements used to produce this map are shown in Figure 4. As discussed previously, the calculated effects of isostatic compensation at a deep crustal-upper mantle interface are removed in the generation of a residual gravity map; this enhances the shallower (<15 km) anomalies. A comparison of Figure 15 with Figure 5 illustrates how the near surface features are enhanced. The gravity anomaly associated with the Weber Basin is better resolved on the residual map than the regional
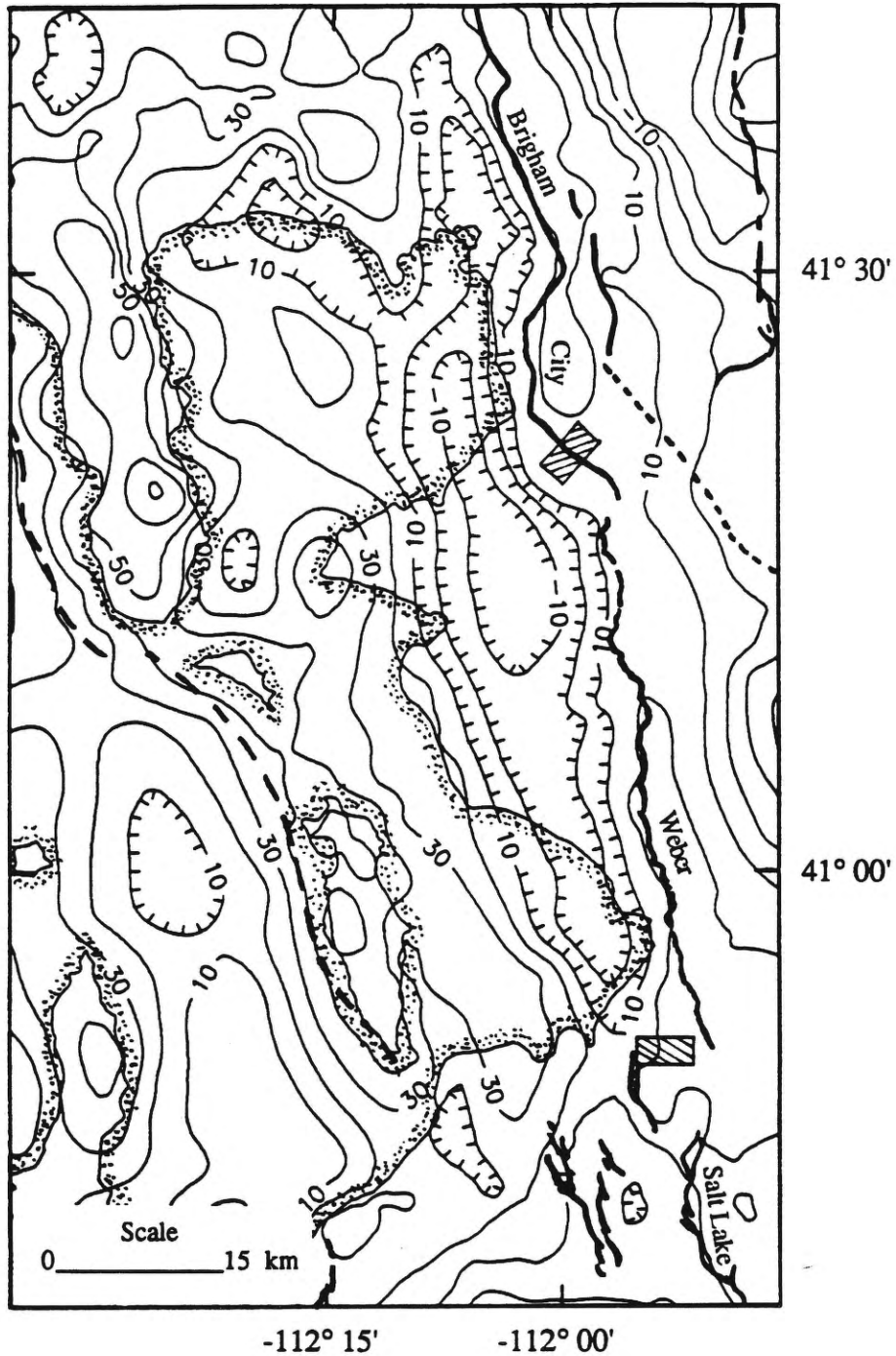
Figure 15. Residual complete Bouguer anomaly gravity contour map of the study area with fault segment boundaries from Machette et al. (1991). Contour interval is 10 mGal.

complete Bouguer anomaly map. From this map two separate types of structural features can be interpreted as follows.

Four Wasatch fault segments (Collinston, Brigham City, Weber and Salt Lake segments as described by Machette et al., (1991) are present in the study area. As can be seen from Figure 15, the gravity contours trend sub-parallel to the surface trace of the Wasatch fault in this study area except at two locations: the Brigham City-Weber and Weber-Salt Lake segment boundaries show a distinct gap between the gravity contours and the mapped fault trace. These perturbations are fairly prominent features on the gravity map. A small gravity field perturbation is associated with the Collinston-Brigham City segment boundary. The gravity expression does not indicate this to be a large asperity on the fault and it is not considered likely to be a persistent segment boundary as defined by Wheeler (1988).

The magnitude of the regional gravity anomaly associated with the basin diminishes south of Bountiful and north of Brigham City. The Salt Lake salient appears to be a continuous basement structure across the basin responsible for the reduced amplitude of the gravity anomaly south of Bountiful. Schwartz and Coppersmith (1984) observed no evidence of paleoseismicity along the Collinston segment over the past 13,500 years. If this is representative of the seismic activity over the lifetime of the segment the relatively small gravity anomaly may be due to languorous basin formation in this area. Also, the gravity anomaly associated with the Weber Basin branches southwest of Brigham City. One branch trends parallel to the Wasatch fault; the other branch trends northwest and cuts across the basement high. No other large scale (>10 km) basement structures such as found by Zoback (1983) were noticed in this study.

Interpretation of Gravity Inversion Results

Numerous investigators have calculated depth-to-basement values for various locations across the basin (Zoback, 1983; Lambert and West, 1989; Glenn et al., 1980;

Wilson et al., 1986). A number of exploratory wells which penetrated basement were drilled by various energy companies. The results of my analysis are compared to the wells and these investigators' depth-to-basement calculations. An interpretation of the basin geometry with respect to the tectonics of the region is also discussed.

Basin depths from the two wells used in this study were not used as constraints for the gravity inversions. Well "a" is located in Model 2 and has been interpreted to penetrate basement at a depth of 1070 meters. The depth-to-basement contour map shows a depth of approximately 1100 to 1300 meters at this location. This depth-to-basement value is associated with the unconstrained model; the result gives confidence to the other depths calculated for Model 2. Well "b" is located in Model 1 and within 1.0 km of seismic profile 7. Three depth values determined from the seismic profiles are located within 2.0 km of well "b" and no gravity inversion nodes are located within 2.5 km of this well. Consequently, the depth value at this location is heavily influenced by the seismic profile and a comparison to depths calculated by the gravity inversion routine is not valid.

A 3.35 km deep well was drilled by Geothermal Kinetics northwest of Brigham City (Figure 16). From well cuttings the well was interpreted to intersect the Wasatch fault at 2.39 km depth which corresponds to a fault dip of about 42° (Morgan, personal communication, 1991). My basin model shows a basin depth of about 1.0 km which does not compare favorably with this above value. The gravity anomaly associated with this area does not indicate such a deep basin contact if the gravity anomaly and corresponding depth are compared to other locations in the basin. The resolution of this part of the basin model may be less than other areas due to the fact that this area is located at the northeast edge of the unconstrained basin model (Model 2).

As might be expected, comparison with other investigators' results were mixed. Lambert and West (1989) conducted a shallow, sparker ("continuous") seismic profiling
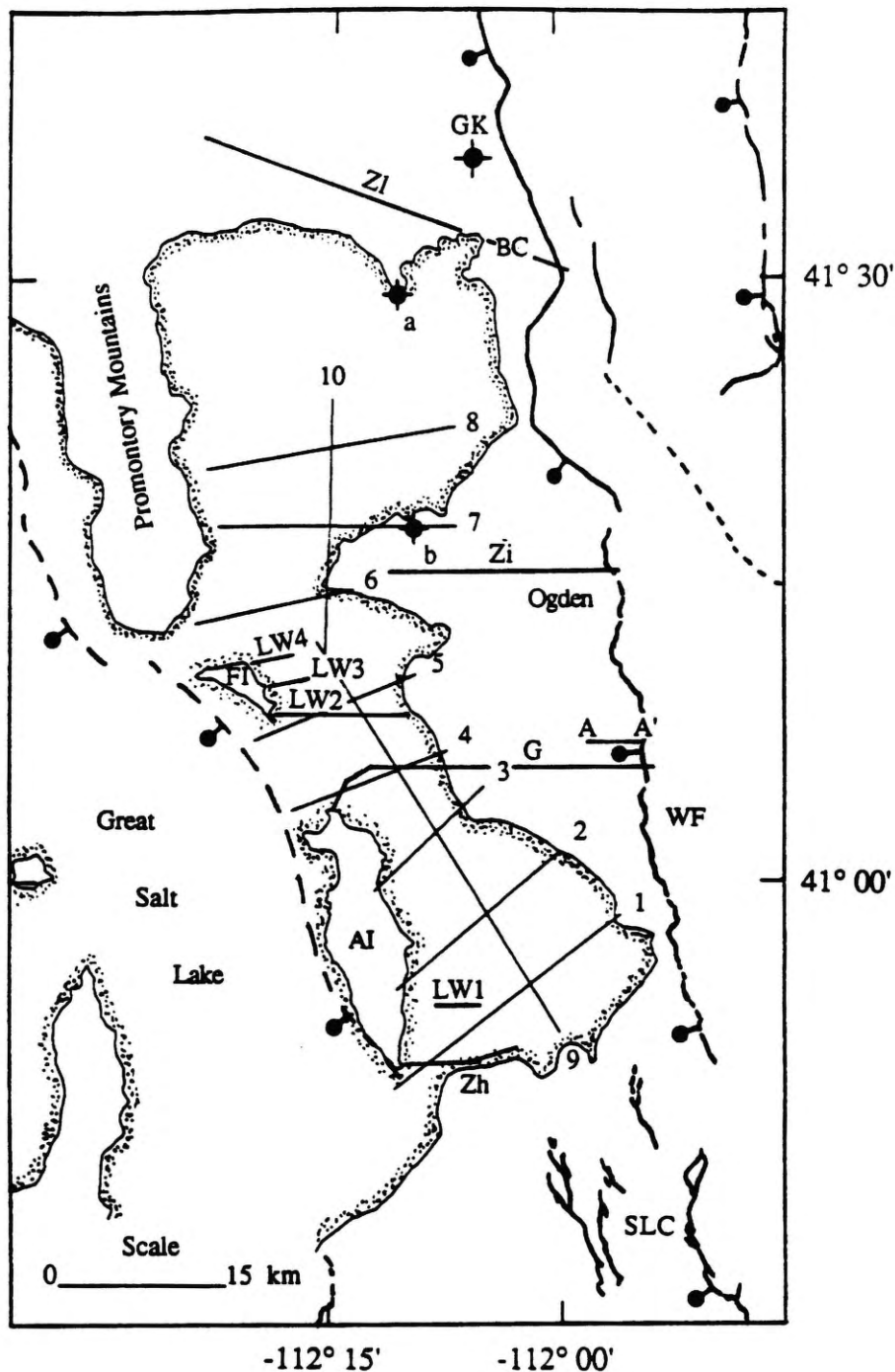
Figure 16. Map showing the locations of other investigators' two-dimensional depth-to-basement profiles which are compared to the results of this study. G = Glen et al. (1980), GK = Geothermal Kinetics, LW = Lambert and West (1989), Z = Zoback (1983), A-A' shows location of seismic reflection profile from Smith and Bruhn (1984).

survey east of Fremont and Antelope islands (Figure 16). The maximum depth of penetration for this method is approximately 300 m. All the calculated depths from their study are located between the 0 and 500 m contours on the depth-to-basement contour map, as one would expect given the depth of penetration of the method.

Wilson et al. (1986) interpreted four seismic profiles, three of which were also used in this study, lines 1, 7 and 8 (Figure 16). The estimated depths beyond the end of seismic profile 1 are deeper by over 1000 m than I observed. But the estimated depth of 2100 m for the west side of the profile is very close (within 200 m) to the values I calculated. The locations and approximate depths of depocenters shown by Wilson et al. (1986) correlate well with the depth-to-basement contour map produced in this study.

Glenn et al. (1980) produced a depth-to-basement profile by using forward modeling of gravity data. The profile trends eastward from the northeastern end of Antelope Island to the Wasatch fault (Figure 16). A density contrast of -0.43 g/cc was used for their modeling. The geometry of the profile matches closely the results of this study. In gravity modeling, a reduction in density contrast between basin sediments and bedrock will result in an increase in volume (depth to the interface). For this reason, the estimated depth of the basin is about 15% greater for the 2-D model because of the smaller density contrast used in the modeling.

Zoback (1983) compiled three 2-D geometry profiles using forward modeling of gravity data in the study area (Figure 16). All three models used a density contrast of -0.5 g/cc. Using her terminology, profile "h" is located at the south end of Antelope Island and trends eastward approximately 10 km. The maximum depth-to-basement associated with this profile is 1.83 km; this value correlates very well with my results. Profile "i" trends eastward from Little Mountain to the Wasatch fault. The maximum basin depth along this profile is 2.59 km. Again, the geometry and depth estimate are consistent with the results of this study. Profile "l" trends east-southeastward from the

Promontory Mountains to Brigham City. The maximum basin depth of 2.10 km agrees to within 300 m of my results. The 2-D geometry along this profile is also consistent with the geometry shown in the depth-to-basement contour map. From the above comparison of depth-to-basement estimates and basin geometries, the studies are remarkably consistent.

The entire Weber segment of the Wasatch fault shows the basement surface dipping 13° to 19° west from the surface trace of the Wasatch fault to the basin bottom. The dip decreases from 19° west in the south to 13° west in the north. This range of dips is consistent with a value of 17° west at Hill Air Force Base determined by Smith and Bruhn (1984) and a value of 18° west at Kaysville calculated by Stephenson (1991). It is not reasonable to assume this represents the dip of the Wasatch fault along the Weber segment. The top of Figure 17 shows the basement reflector (?) interpreted by Smith and Bruhn (1984) and the bottom of the figure illustrates my fault geometry model for the Weber segment of the Wasatch fault. Smith (1984) modeled the effects of this type of fault geometry on seismic reflection imaging. The top of Figure 18 shows one of Smith's (1984) fault models and the bottom of the figure shows the corresponding seismic reflection profile. At shallow dips a near continuous reflection is produced by this fault geometry which is similar to the reflection shown by Smith and Bruhn (1984).

Smith and Bruhn (1984) and later Anderson (1989) postulated that the late Cenozoic normal faulting and basin geometry are influenced by Early and Pre-Cenozoic structures. The structures of interest in this study are the Absaroka ramp-anticline, the Willard-Paris thrust sheet, the Ogden thrust zone and the Salt Lake salient. Eardley (1944) speculated, after studying the Ogden thrust zone and Willard-Paris thrust sheet, these structures influenced the geometry of the Wasatch fault between Ogden and Brigham City. Eardley's (1944) speculation is the most reasonable explanation for the

Wasatch Fault

A

A'

TIME (s)

0.0

1.0

2.0

3.0

4.0

5.0

0   1   2   3 KM

0   1   2   3 MI

Surface

Sediment

18°   40°
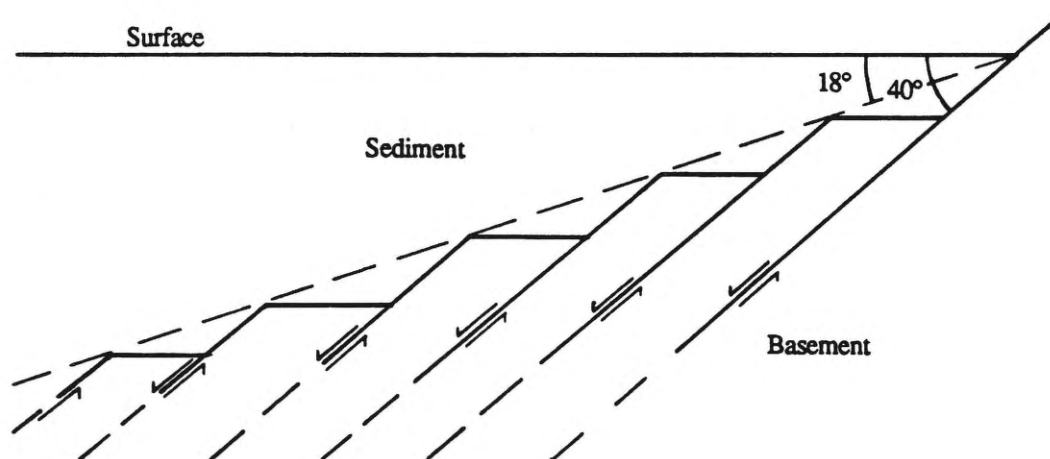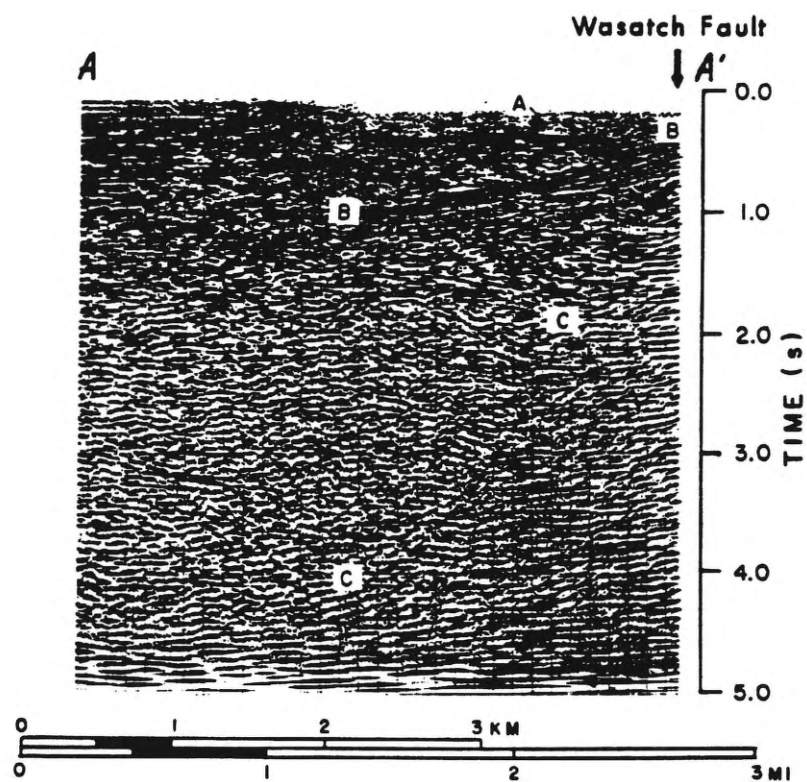
Basement

Figure 17. Seismic reflection profile from Smith and Bruhn (1984) showing the basement reflector dipping 17° west (top) and model for this geometry (bottom).
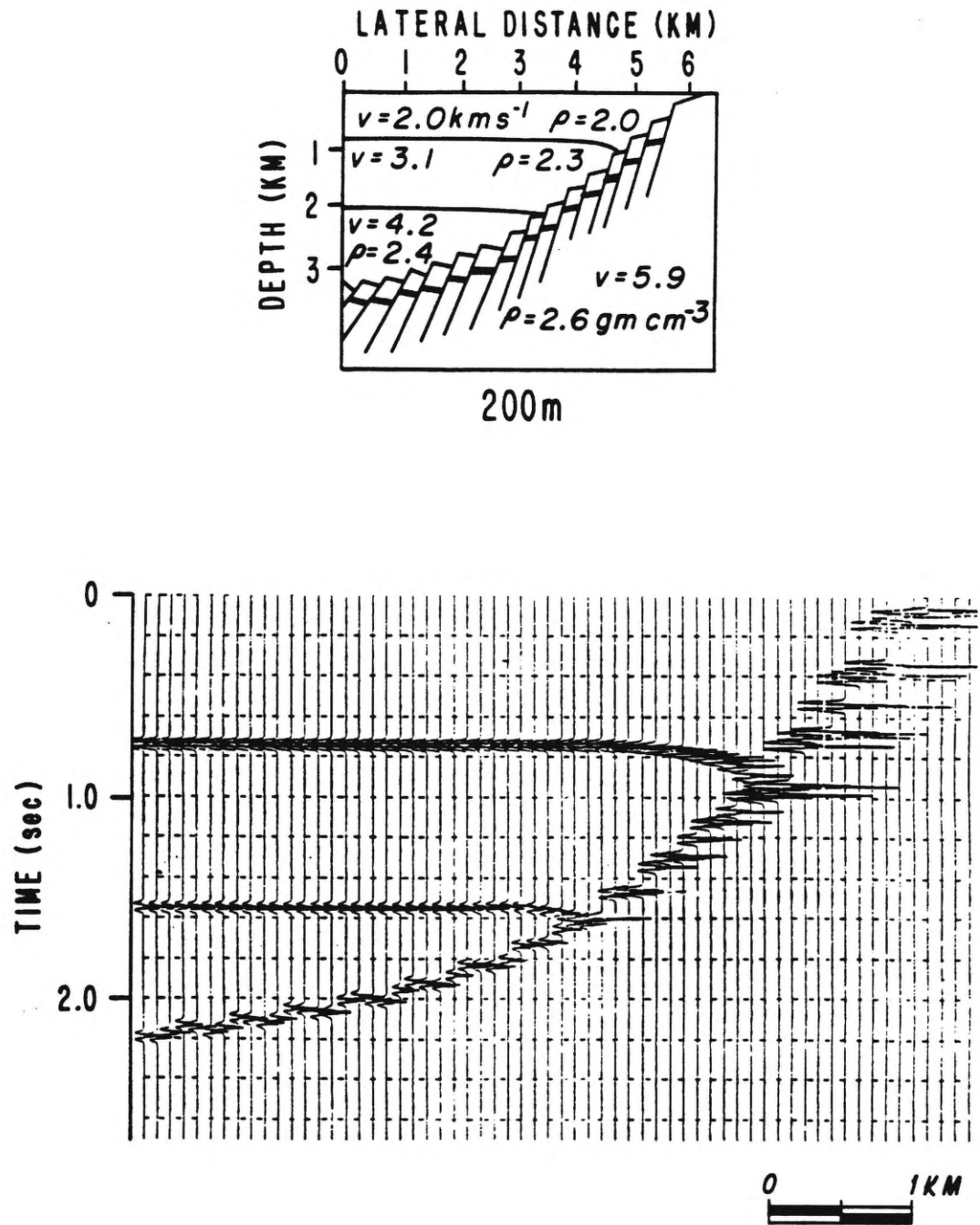
Figure 18. Acoustic velocity and density model for fault geometry discussed in text (top) from Smith (1984) and corresponding synthetic reflection seismic profile (bottom).

change in geometry of the Wasatch fault north of Ogden. The Salt Lake salient is the western boundary between the north-south oriented ramp-anticline and the east-west oriented Uinta Arch. This area has a complex structural history as can be seen from the geologic map of the area by Bryant (1990) . The Salt Lake salient is located where the dominant structure orientation rotates from north-south to east-west. This change in orientation is most probably responsible for the change in geometry of the Wasatch fault at the southern end of the Weber segment.

The axis of the Absaroka ramp-anticline trends sub-parallel to the Weber segment of the Wasatch fault. This is the major structural feature east of the Wasatch fault over this region. The ramp-anticline is presumed to have been active 90 to 50 m.y.b.p. (Yonkee, 1990). Considering this anticline was formed because of compressional stresses, the major component of the maximum principal stress, σ_1, was oriented east-west during this period. Assuming this is also the direction of maximum shortening, foliation is produced perpendicular to this direction, or sub-parallel to the axial surface of the fold (Park, 1983). Ramsay (1967, p.401) discusses the possibility of forming conjugate shear planes in the core of anticlines. This is a plausible explanation for the origin of the Francis Peak fault zone considering this is the assumed culmination of the ramp-anticline (Yonkee, 1990).

Rogers and Rizer (1981) model antithetic and synthetic secondary faults associated with thrust faulting. According to their models, secondary faults occur in both the hanging wall and footwall. These secondary faults are oriented subparallel to the strike of the master thrust fault. Bryant (1984) shows a whole series of faults oriented subparallel to both the Weber segment of the Wasatch fault and the axis of the Absaroka ramp-anticline. No sense of movement is shown for these faults. It is reasonable to assume these faults are associated with the thrusting which formed the Absaroka ramp-anticline, i.e., formed as secondary faults produced by the thrusting.

From approximately 50 to 15 m.y.b.p. the orientation of σ_1 had change from east-west to vertical to allow normal faulting along the Wasatch fault. Also, for normal faulting the minimum principal stress, σ_3, is oriented subperpendicular to the strike of the fault, which in this case is east-west. The current stress field orientation is optimal to take advantage of the preexisting zones of weakness discussed above. The most plausible geometry to explain the shallow dip of the basement along the Weber segment is a series of normal faults down-stepping to the basin bottom. This interpretation is consistent with the seismic interpretation, but in this case the geometry is seen at the sediment-basement contact.

The depth-to-basement contour map shows a depression of 5.0 to 5.5 km between North Ogden and Brigham City; the question is, is it really that deep? Three lines of evidence suggest it is. First, the calculated dip from the surface trace of the Wasatch fault to the deepest part of the hole is approximately 40°. This value is quite respectable for a normal fault. Second, the Utah Valley and Great Salt Lake basin show comparable depths. A 4.05 km well drilled by Gulf Oil west of Spanish Fork in southern Utah Valley bottomed out in Miocene sediments (Hintze, 1988). Two wells drilled by Amoco Oil west of the Promontory Mountains in the Great Salt Lake recorded Miocene sediments to depths over 3.75 km. One well penetrates Precambrian basement, the other does not. Third, the magnitude of the gravity anomalies over these areas are similar. The gravity anomalies associated with the wells in Utah Valley and the west side of the Great Salt Lake are approximately 35 mGals. The anomaly associated with the hole in this study area is approximately 40 mGals. These values vary somewhat (within about 5 mGals) depending on the regional removed from the gravity data.

There are, however, two arguments against the depression being as deep as shown. First, a fundamental assumption for the gravity inversion is to assume a homogeneous density contrast across the study area. If the density contrast varies

laterally across the hole, which is a possibility, the density contrast used in the gravity inversion will not accurately represent the density contrast of the depression and this will add a fictitious component to the depth-to-basement estimate. For this case, if the density of the sediments in the hole is less than the density of the surrounding sediments the hole will appear deeper. Second, the gravity data coverage in this area may not be dense enough to accurately resolve this part of the model. Fewer gravity values are located in this section than in most other parts of the model.

It is quite reasonable to assume the depression is deeper than the rest of the basin. Whether it is 0.5 km deeper or 2.0 km deeper is indeterminate from the available data. Also, the northern edge of the depression coincides with the seam between the two models. Model edge effects could partially alter the geometry of this side of the depression as well.

The implications of the hole are substantial. The southern half of the hole is located west of the Brigham City-Weber segment boundary; the northern end is located near the middle of the Brigham City segment. Considering the segment boundaries are rupture boundaries along the fault, and the greatest amount of offset along the Wasatch fault is in the deepest part of the basin, the current segment boundaries do not accurately represent the long term (> 10,000 yrs.(?)) segment boundaries associated with the fault. This implies some or all of the current segment boundaries are transitory over the lifetime of the fault (Bruhn, personal communication, 1991). This interpretation is strikingly different than interpretations by Machette et al. (1991) and Schwartz and Coppersmith (1984). This interpretation also puts an upper bound on what Wheeler (1988) classifies as persistent segment boundaries.

CONCLUSIONS

The depth-to-basement contour map produced in this study shows basin depths and geometries which closely match (differ by < 15% in all cases) the four 2-D profiles produced by other investigators (Zoback, 1983; and Glenn et al., 1980). These four profiles are distributed throughout the study area from the north of Brigham City to the southeast of Antelope Island. Considering that the basin geometry varies between these profiles because of 3-D variations in the basin, and the results of this study are consistent with the profiles, it is reasonable to assume the contour map accurately maps these variations throughout the basin. Therefore, we believe the contour map accurately represents the geometry of the basin.

The basin geometry elucidated by the depth-to-basement contour map implies the segments of the Wasatch fault in the study area are affected by Early and Pre-Cenozoic structures, i.e., the Absaroka ramp-anticline, the Salt Lake salient and the thrust sheets north of Ogden. The complex geometries of the thrust sheets north of Ogden are at least partly responsible for the change in orientation of the Wasatch fault in this area. It is not very likely a coincidence that the Wasatch fault geometry changes at the Salt Lake salient which is the northwestern end of the Uinta Arch. The fault geometry along the Weber segment is strongly influenced by the Absaroka ramp-anticline and the zones of weakness (secondary faults, foliation and conjugate shear planes) associated with this structure. The rotation in the stress field from compression during the Sevier Orogeny to the present extensional stress field orientation allows the normal faulting to take advantage of these zones of weakness. The geometry along this segment is modeled by a series of en echelon normal faults down-stepping from the surface traces of the Wasatch fault basinward. If the Wasatch fault zone is not an extraordinary case,

preexisting structures, thrust sheets, large-scale folds, igneous intrusions, etc., are most likely the origin of large scale (>10 km^2) asperities along major fault systems.

If the depression in the basin between Ogden and Brigham City is real, the notion of persistent segment boundaries in this area has to be rethought, because the southern portion of the deep spot is located at a segment boundary as mapped by Machette et al. (1991). Segment boundaries are thought to be barriers to fault rupture propagation. This implies the ends are basically fixed with respect to the rest of the segment and the displacement along the segment diminishes toward the ends. The southern half of the deep spot is located west of the mapped boundary between the Brigham City and Weber segments. It is difficult to explain having the maximum offset on the fault (deepest part of the basin) at this location if these boundaries are persistent over geologically significant time scales (>10,000 yrs.(?)). This result implies segment boundaries are transitory over the lifetime of the fault system.

The major factors associated with earthquake hazard analysis are source effects (location, magnitude and focal mechanism of earthquake), path, and site amplification effects. Site amplification analysis includes estimation of effects from seismic energy focusing and channeling, and basin resonance. A dominant factor which controls low frequency amplification effects is basin geometry. The basin geometry strongly influences the location and strength of amplification effects in the basin. The basin model produced in this study can be used in site amplification investigations. Considering the region from Bountiful to Brigham City is one of the most highly populated areas in the state, knowledge of these effects will be very important for future urban planning and emergency preparation.

The geometry of the Weber Basin is significantly different than the geometry of the Great Salt Lake Basin shown by Viveiros (1986). Viveiros' (1986) basin model shows an asymmetric basin geometry with a shallow eastward dip of approximately 12°

to 15° from Stansbury and Carrington islands to the deepest (> 3.0 km) part of the basin. The east side of the basin is bounded by a west dipping listric normal fault with about 3 to 4 km of offset (Figure 19). The Weber Basin model shows a broad nearly flat basement high projecting eastward from Antelope Island to halfway across the basin. The sediment-basement contact then dips about 30° east to the basin bottom. From the surface of the Wasatch fault, the sediment-basement contact dips at about 15° to 20° west into the basin. A series of en echelon normal faults down-stepping from the surface traces of the Wasatch fault basinward explains this shallow dip. The difference between the two basin geometries is illustrated in Figure 19.
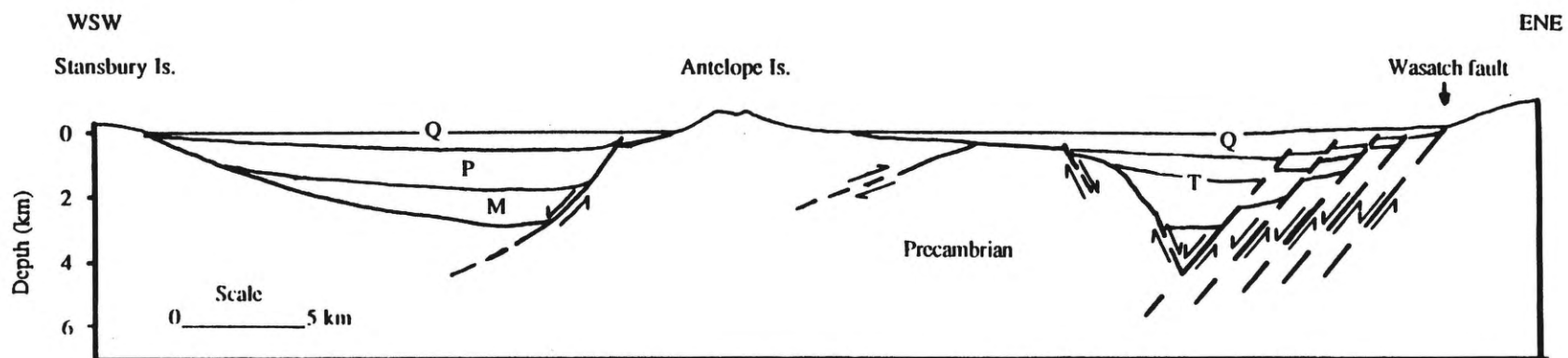
Figure 19. Generalized cross-section from Stansbury Island to the Wasatch Front showing the difference in geometry between the Great Salt Lake and Weber basins. T = Tertiary, M = Miocene, P = Pliocene, Q = Quaternary.

APPENDIX

Table 3

Longitude, Latitude both in Decimal Degrees, and Depth of Basin Model

Longitude	Latitude	Depth (m)
-112.1760	40.8320	385.00
-112.1700	40.8355	245.00
-112.1640	40.8390	230.00
-112.1570	40.8423	350.00
-112.1510	40.8456	635.00
-112.1460	40.8489	785.00
-112.1390	40.8526	1135.00
-112.1330	40.8560	1220.00
-112.1270	40.8595	1790.00
-112.1210	40.8628	1980.00
-112.1150	40.8664	2350.00
-112.1080	40.8701	1985.00
-112.1020	40.8732	1830.00
-112.0960	40.8767	1325.00
-112.0900	40.8801	885.00
-112.0840	40.8837	295.00
-112.0770	40.8870	185.00
-112.0710	40.8906	220.00
-112.0650	40.8941	160.00
-112.0590	40.8975	190.00
-112.0530	40.9007	180.00
-112.0470	40.9044	270.00
-112.0400	40.9076	375.00
-112.0340	40.9113	420.00
-112.0270	40.9149	430.00
-112.0220	40.9178	390.00
-112.0160	40.9214	545.00
-112.0090	40.9251	750.00
-112.0030	40.9283	1050.00
-111.9980	40.9314	1575.00
-111.9910	40.9349	2220.00
-111.9850	40.9386	2455.00
-111.9790	40.9424	3200.00
-111.9720	40.9455	3465.00
-112.1660	40.9162	0.00
-112.1590	40.9208	0.00
-112.1520	40.9251	113.00
-112.1440	40.9304	175.50

Longitude	Latitude	Depth (m)
-112.1360	40.9350	181.42
-112.1290	40.9395	214.13
-112.1210	40.9442	267.72
-112.1140	40.9487	288.51
-112.1070	40.9531	282.72
-112.1000	40.9576	343.69
-112.0920	40.9621	288.69
-112.0850	40.9668	254.96
-112.0780	40.9714	236.71
-112.0710	40.9757	252.70
-112.0670	40.9776	260.58
-112.0600	40.9824	401.79
-112.0520	40.9869	613.09
-112.0450	40.9916	810.16
-112.0370	40.9960	1112.72
-112.0300	41.0003	1497.19
-112.0230	41.0048	2024.25
-112.0150	41.0094	2514.56
-112.0080	41.0141	2570.31
-112.0010	41.0183	2632.78
-112.1900	41.0000	110.00
-112.1800	41.0073	460.00
-112.1760	41.0099	660.00
-112.1690	41.0149	985.00
-112.1610	41.0198	1380.00
-112.1540	41.0252	1530.00
-112.1470	41.0300	1130.00
-112.1400	41.0351	1130.00
-112.1330	41.0400	980.00
-112.1260	41.0452	520.00
-112.1180	41.0502	520.00
-112.1110	41.0553	520.00
-112.1040	41.0601	600.00
-112.0970	41.0651	630.00
-112.0900	41.0702	830.00
-112.2760	41.0644	0.00
-112.2670	41.0668	0.00
-112.2580	41.0696	0.00
-112.2490	41.0722	0.00
-112.2400	41.0750	79.30
-112.2310	41.0774	382.50
-112.2220	41.0800	660.00
-112.2130	41.0825	744.80
-112.2040	41.0852	826.80
-112.1950	41.0877	796.10
-112.1860	41.0904	622.80
-112.1760	41.0931	744.30
-112.1680	41.0956	729.70
-112.1590	41.0981	647.50
-112.1500	41.1009	654.70
-112.1410	41.1034	646.90

Longitude	Latitude	Depth (m)
-112.1320	41.1058	625.20
-112.3290	41.1204	0.00
-112.3210	41.1232	0.00
-112.3110	41.1262	0.00
-112.3030	41.1288	80.00
-112.2930	41.1315	185.00
-112.2850	41.1342	370.00
-112.2750	41.1370	425.00
-112.2660	41.1399	205.00
-112.2570	41.1424	180.00
-112.2480	41.1452	180.00
-112.2400	41.1478	925.00
-112.2310	41.1503	1725.00
-112.2240	41.1526	1560.00
-112.2150	41.1552	1490.00
-112.2060	41.1579	1275.00
-112.1970	41.1606	1120.00
-112.1890	41.1632	930.00
-112.1790	41.1662	890.00
-112.2670	41.1869	230.00
-112.2620	41.1816	210.00
-112.2570	41.1755	260.00
-112.2520	41.1698	255.00
-112.2460	41.1634	375.00
-112.2420	41.1577	890.00
-112.2360	41.1518	1250.00
-112.2310	41.1458	920.00
-112.2260	41.1401	305.00
-112.2200	41.1338	420.00
-112.2150	41.1278	830.00
-112.2100	41.1219	1290.00
-112.2040	41.1160	1155.00
-112.1990	41.1102	785.00
-112.1940	41.1040	720.00
-112.1890	41.0982	1000.00
-112.1830	41.0923	647.00
-112.1780	41.0862	565.00
-112.1730	41.0803	450.00
-112.1680	41.0744	605.00
-112.1620	41.0687	650.00
-112.1570	41.0625	755.00
-112.1520	41.0568	1000.00
-112.1470	41.0510	1030.00
-112.1410	41.0449	1115.00
-112.1360	41.0392	980.00
-112.1310	41.0329	410.00
-112.1260	41.0266	410.00
-112.1200	41.0205	385.00
-112.1150	41.0146	250.00
-112.1090	41.0084	245.00
-112.1040	41.0021	300.00

Longitude	Latitude	Depth (m)
-112.0980	40.9958	205.00
-112.0930	40.9899	325.00
-112.0870	40.9837	415.00
-112.0820	40.9776	290.00
-112.0770	40.9714	235.00
-112.0710	40.9653	250.00
-112.0660	40.9591	345.00
-112.0600	40.9529	415.00
-112.0550	40.9469	425.00
-112.0490	40.9409	350.00
-112.0440	40.9346	545.00
-112.0390	40.9286	635.00
-112.0340	40.9223	505.00
-112.0280	40.9163	335.00
-112.0230	40.9101	525.00
-112.0170	40.9038	490.00
-112.0120	40.8978	475.00
-112.0070	40.8913	455.00
-112.0010	40.8855	375.00
-112.4120	41.2154	0.00
-112.4040	41.2167	81.28
-112.3940	41.2183	714.07
-112.3860	41.2195	1272.24
-112.3680	41.2223	1966.34
-112.3590	41.2238	1967.72
-112.3500	41.2251	1927.47
-112.3400	41.2266	1842.83
-112.3310	41.2282	1677.96
-112.3220	41.2295	1344.23
-112.3120	41.2310	1382.93
-112.3020	41.2324	825.83
-112.2930	41.2338	419.21
-112.2840	41.2352	231.10
-112.2750	41.2366	146.40
-112.2670	41.2379	0.00
-112.2580	41.2392	0.00
-112.2420	41.2418	0.00
-112.3870	41.2945	180.00
-112.3770	41.2945	520.00
-112.3670	41.2945	840.00
-112.3570	41.2946	1565.00
-112.3480	41.2945	1680.00
-112.3380	41.2945	1460.00
-112.3280	41.2945	565.00
-112.3180	41.2944	955.00
-112.3080	41.2943	1410.00
-112.2990	41.2945	1575.00
-112.2880	41.2944	1145.00
-112.2790	41.2945	1155.00
-112.2690	41.2945	755.00
-112.2590	41.2945	365.00

Longitude	Latitude	Depth (m)
-112.2490	41.2946	260.00
-112.2390	41.2944	175.00
-112.2300	41.2943	85.00
-112.2200	41.2943	180.00
-112.2100	41.2943	310.00
-112.2010	41.2942	385.00
-112.1910	41.2944	630.00
-112.1810	41.2943	770.00
-112.1710	41.2941	720.00
-112.1610	41.2942	1085.00
-112.1520	41.2941	1305.00
-112.1410	41.2941	1310.00
-112.4050	41.3443	120.00
-112.3940	41.3456	270.00
-112.3850	41.3467	440.00
-112.3750	41.3479	600.00
-112.3650	41.3491	770.00
-112.3560	41.3504	895.00
-112.3460	41.3516	1010.00
-112.3360	41.3531	475.00
-112.3270	41.3540	320.00
-112.3160	41.3551	260.00
-112.3080	41.3563	430.00
-112.2980	41.3575	1910.00
-112.2880	41.3585	1860.00
-112.2790	41.3599	1922.00
-112.2690	41.3607	1525.00
-112.2600	41.3620	1355.00
-112.2510	41.3631	550.00
-112.2410	41.3643	770.00
-112.2320	41.3656	1350.00
-112.2220	41.3666	1450.00
-112.2130	41.3678	1305.00
-112.2030	41.3690	975.00
-112.1950	41.3700	820.00
-112.1850	41.3711	850.00
-112.1750	41.3724	1345.00
-112.1660	41.3735	1370.00
-112.1570	41.3745	1835.00
-112.1470	41.3757	2040.00
-112.1380	41.3769	2125.00
-112.2950	41.3987	996.65
-112.2940	41.3910	1628.23
-112.2920	41.3843	2842.15
-112.2910	41.3764	2302.63
-112.2890	41.3695	2357.74
-112.2880	41.3623	1996.76
-112.2870	41.3550	1732.31
-112.2850	41.3481	1554.76
-112.2840	41.3405	1513.56
-112.2830	41.3336	1410.32

Longitude	Latitude	Depth (m)
-112.2810	41.3264	1228.87
-112.2800	41.3192	1116.91
-112.2800	41.3125	1197.54
-112.2790	41.3053	1093.44
-112.2800	41.2983	984.29
-112.2790	41.2913	1061.54
-112.2790	41.2880	977.20
-112.2780	41.2808	796.70
-112.2770	41.2736	651.30
-112.2770	41.2663	612.30
-112.2760	41.2589	629.89
-112.2760	41.2517	529.99
-112.2750	41.2441	287.71
-112.2740	41.2372	164.90
-112.2740	41.2299	79.20
-112.2740	41.2222	278.41
-112.2740	41.2154	486.47
-112.2740	41.2079	586.72
-112.2740	41.2012	526.48
-112.2730	41.1938	388.22
-112.0260	41.4602	0.00
-112.0270	41.4076	0.00
-111.9960	41.3600	0.00
-111.9340	41.3201	0.00
-111.9480	41.2731	0.00
-111.9300	41.2177	0.00
-111.9310	41.1631	0.00
-111.9030	41.1245	0.00
-111.9050	41.0623	0.00
-111.8930	41.0176	0.00
-111.8790	40.9800	0.00
-111.8700	40.9413	0.00
-111.8440	40.8901	0.00
-111.8710	40.8471	0.00
-111.9070	40.8146	0.00
-111.8520	40.7872	0.00
-112.4400	41.4552	0.00
-112.4330	41.4192	0.00
-112.4280	41.3897	0.00
-112.4270	41.3547	0.00
-112.4020	41.3267	0.00
-112.3960	41.2707	0.00
-112.4090	41.2404	0.00
-112.4400	41.2122	0.00
-112.3620	41.1790	0.00
-112.3400	41.1820	0.00
-112.3170	41.1502	0.00
-112.2370	41.0582	0.00
-112.2080	41.0388	0.00
-112.1900	41.0212	0.00
-112.1700	40.9553	0.00

Longitude	Latitude	Depth (m)
-112.1720	40.9193	0.00
-112.1710	40.8900	0.00
-112.1730	40.8618	0.00
-111.9560	40.8902	3290.00
-111.9220	40.9085	950.00
-111.8930	40.9255	90.00
-111.9700	40.9412	8670.00
-111.9400	40.9558	1390.00
-111.9070	40.9722	370.00
-111.9810	40.9822	2960.00
-111.9510	40.9952	1480.00
-111.9120	41.0106	50.00
-111.9900	41.0239	2050.00
-111.9560	41.0368	1130.00
-111.9160	41.0510	0.00
-112.0320	41.0582	2920.00
-111.9970	41.0678	1570.00
-111.9530	41.0799	590.00
-112.0700	41.0899	2050.00
-112.0290	41.0984	2230.00
-111.9910	41.1071	1900.00
-111.9390	41.1184	490.00
-112.1080	41.1288	1420.00
-112.0650	41.1354	2160.00
-112.0220	41.1410	2090.00
-111.9790	41.1468	790.00
-111.9280	41.1542	140.00
-112.0970	41.1733	3580.00
-112.0530	41.1758	3640.00
-112.0060	41.1784	2740.00
-111.9580	41.1805	340.00
-112.1250	41.2057	3890.00
-112.0780	41.2060	2510.00
-112.0310	41.2067	2920.00
-111.9780	41.2077	1250.00
-112.1010	41.2484	1870.00
-112.0550	41.2480	2270.00
-112.0030	41.2469	1960.00
-111.9550	41.2462	520.00
-112.1230	41.2896	1970.00
-112.0770	41.2896	2160.00
-112.0280	41.2884	1770.00
-111.9800	41.2884	590.00
-112.0980	41.3232	6250.00
-112.0510	41.3226	1900.00
-112.0030	41.3222	530.00
-111.9570	41.3213	450.00
-112.1230	41.3598	3740.00
-112.0700	41.3597	1280.00
-112.0220	41.3596	0.00
-112.1470	41.3982	2850.00

Longitude	Latitude	Depth (m)
-112.0980	41.3988	5480.00
-112.0490	41.3990	580.00
-112.4320	41.3956	0.00
-112.3710	41.3962	1840.00
-112.3200	41.3964	1460.00
-112.2050	41.3973	750.00
-112.0010	41.3997	0.00
-112.4540	41.4408	0.00
-112.4010	41.4408	250.00
-112.3440	41.4401	2010.00
-112.2880	41.4399	0.00
-112.2320	41.4393	390.00
-112.1740	41.4390	1270.00
-112.1220	41.4387	0.00
-112.0270	41.4382	0.00
-112.4280	41.4794	100.00
-112.3160	41.4781	260.00
-112.2580	41.4782	1300.00
-112.2030	41.4778	1550.00
-112.1460	41.4771	360.00
-112.0970	41.4766	2360.00
-112.0490	41.4759	710.00
-112.0040	41.4753	0.00
-112.4580	41.5184	100.00
-112.2880	41.5167	4680.00
-112.2320	41.5161	680.00
-112.1770	41.5157	660.00
-112.1230	41.5153	640.00
-112.0730	41.5146	1650.00
-112.0250	41.5139	40.00
-112.3160	41.5563	3630.00
-112.2620	41.5556	1730.00
-112.2040	41.5549	0.00
-112.1510	41.5546	830.00
-112.0990	41.5543	1830.00
-112.0520	41.5536	1450.00
-112.0020	41.5532	0.00
-112.3450	41.5955	540.00
-112.2290	41.5938	0.00
-112.1770	41.5940	0.00
-112.1270	41.5930	1560.00
-112.0340	41.5923	0.00
-112.4800	41.6368	0.00
-112.3740	41.6350	0.00
-112.3170	41.6345	320.00
-112.2560	41.6336	50.00
-112.2050	41.6329	140.00
-112.1510	41.6320	790.00
-112.1030	41.6320	1090.00
-112.0570	41.6304	0.00

REFERENCES

Anderson, R. E., 1989, Tectonic evolution of the Intermontane System; Basin and Range, Colorado Plateau, and High Lave Plains, *in* Pakiser, L. C., and Mooney, W. D., Eds., Geophysical framework of the continental United States: Geol. Soc. Am. Memoir 172, The Geological Society of America, Inc., 163–176.

Arabasz, W. J., Pechmann, J. C., and Brown, E. D., 1987, Observational seismology and evaluation of earthquake hazards and risk in the Wasatch Front area, Utah: *in* Gori, P. L., and Hays, W. W., Eds., Assessment of regional earthquake hazards and risk along the Wasatch Front, Utah, Vol.1: U. S. Geol. Surv. Prof. Paper 87–585, D1–39 [revised and in press, 1991, U. S. Geol. Surv. Prof. Paper 1500–C].

Arnow, T., and Mattick, R. E., 1968, Thickness of valley fill in the Jordan Valley east of the Great Salt Lake, Utah: U. S. Geol. Surv. Prof. Paper **600-B**, B79–B82.

Barnett, C. T., 1976, Theoretical modeling of the magnetic and gravitational fields of an arbitrarily shaped three-dimensional body: Geophysics, **41**, 1353–1364.

Bryant, B., 1984, Reconnaissance geologic map of the Precambrian Farmington Canyon Complex and surrounding rocks in the Wasatch Mountains between Ogden and Bountiful, Utah: U. S. Geol. Surv., Map I–1447.

Bryant, B., 1990, Geologic map of the Salt Lake City 30' x 60' quadrangle, north-central Utah, and Uinta County, Wyoming: U. S. Geol. Surv., Map 1–1944.

Cook, K. C., Bankey, V., Mabey, D. R., and DePangher, M., 1989, Complete Bouguer gravity anomaly map of Utah: Utah Geol. and Mineral Surv., Map 122.

Cordell, L., Zorin, Y. A., and Keller, G. R., 1991, The decompensative gravity anomaly and deep structure of the region of the Rio Grande Rift: J. Geophys. Res., **96**, 6557–6568.

Davis, F. D., 1985, Geologic map of the northern Wasatch Front, Utah: Utah Geol. and Mineral Surv., Map 53–A.

Eardley, A. J., 1944, Geology of the north-central Wasatch Mountains, Utah: Bull., Geol. Soc. Am., **55**, 819–894.

Fuchs, K. and Muller, G., 1971, Computation of synthetic seismograms with the reflectivity method and comparison with observations: Geophysical Journal of the Royal Astronomical Society, **23**, 417–433.

Glenn, W. E., Chapman, D. S., Foley, D., Capuano, R. M., Cole, D., Sibbett, B., and Ward, S. H., 1980, Geothermal exploration program Hill Air Force Base, Davis and Weber County, Utah: Earth Science Laboratory, University of Utah Research Institute, Prepared for the Department of Energy, Division of Geothermal Energy Contract No. DE–AC07–78ET–28392.

Hill, J. A., 1988, A finite difference simulation of seismic wave propagation and resonance in Salt Lake Valley, Utah: M. S. thesis, University of Utah.

Hintze, L. F., 1980, Geologic map of Utah: Utah Geol. and Mineral Surv.

Hintze, L. F., 1988, Geologic history of Utah: Kowallis, B. J., Ed, Brigham Young Univ. Geol. Studies Special pub. 7.

Lambert, P. M., and West, J. C., 1989, Continuous seismic-reflection survey of the Great Salt Lake, Utah–east of Antelope and Fremont islands: U. S. Geol. Surv., Water-Resources Investigations Report 88–4157.

Litinsky, V. A., 1989, Concept of effective density: key to gravity depth determinations for sedimentary basins: Geophysics, **54**, 1474–1482.

Machette, M. N., Personius, S. F., Nelson, A. R., Schwartz, D. P., and Lund, W. R., 1991, The Wasatch fault zone, Utah–segmentation and history of Holocene earthquakes: Journal of Structural Geology, **13**, no. 2, 137–149.

Menke, W., 1984, Geophysical data analysis: discrete inverse theory: Academic Press, Inc.

Olson, R. H., 1960, Geology of the Promontory Range, Box Elder county, Utah: Ph.D. dissertation, University of Utah.

Park, R. G., 1983, Foundations of structural geology: Blackie & Son Ltd.

Radkins, H. C., 1990, Bedrock topography of the Salt Lake Valley, Utah, from constrained inversion of gravity data: M. S. thesis, University of Utah.

Ramsay, J. G., 1967, Folding and fracturing of rocks: McGraw-Hill Book Co. (Div. of McGraw-Hill, Inc.).

Richardson, R. M., and MacInnes, S. C., 1989, The inversion of gravity data into three-dimensional polyhedral models: J. of Geophys. Res., **94**, 7555–7562.

Rogers, D. A., and Rizer, W. D., 1981, Deformation and secondary faulting near the leading edge of a thrust fault, *in* McClay, K. R., and Price, N. J., Eds., Thrust and nappe tectonics: Geol. Soc. London, Blackwell Scientific Publications, Inc., 65–77.

Schwartz, D. P., and Coppersmith, K. J., 1984, Fault behavior and characteristic earthquakes: examples from the Wasatch and San Andreas fault zones: J. Geophys. Res., **89**, 5681–5698.

Simpson, R. W., Jachens, R. C., Blakely, R. J., and Saltus, R. W., 1986, A new isostatic residual gravity map of the conterminous United States with a discussion on the significance of isostatic residual anomalies: J. Geophys. Res., **91**, 8348–8372.

Smith, K. A., 1984, Normal faulting in an extensional domain: constraints from seismic reflection interpretation and modeling: M. S. thesis, University of Utah.

Smith, R. B., and Bruhn, R. L., 1984, Intraplate extensional tectonics of the eastern basin-range: inferences on structural style from seismic reflection data, regional tectonics, and thermal-mechanical models of brittle-ductile deformation: J. Geophys. Res., **89**, 5733–5762

Snay, R. A., Smith, R. B., and Soler, T., 1984, Horizontal strain across the Wasatch Front near Salt Lake City, Utah: J. Geophys. Res., **89**, 1113–1122.

Stokes, W. L., 1986, Geology of Utah: Utah Museum of Natural History, University of Utah and Utah Geological and Mineral Survey Department of Natural Resources.

Stephenson, W. J., 1991, High-resolution seismic imaging and gravity analysis of deformation across the Wasatch fault, Kaysville, Utah: M. S. thesis, University of Utah.

Turcotte, D. L., and Schubert, G., 1982, Geodynamics: John Wiley & Sons, Inc.

Viveiros, J. J., 1986, Cenozoic tectonics of the Great Salt Lake from seismic reflection data: M. S. thesis, University of Utah.

Wheeler, R. L., 1988, Persistent segment boundaries on basin-range normal faults: U. S. Geol. Surv. Open-File Report 89-315, 432–444.

Wilson, E. A., Saugy, L., and Zimmermann, M. A., 1986, Cenozoic tectonics and sedimentation of the eastern Great Salt Lake area, Utah: Bull. Soc. Geol. Fr., n° 5, 777–782.

Yonkee, W. A., 1990, Geometry and mechanics of basement and cover deformation, Farmington Canyon Complex, Sevier orogenic belt, Utah: Ph.D. dissertation, University of Utah.

Zoback, M. L., 1983, Structure and Cenozoic tectonism along the Wasatch fault zone, Utah: Mem. Geol. Soc. Am. 157, 3–27.
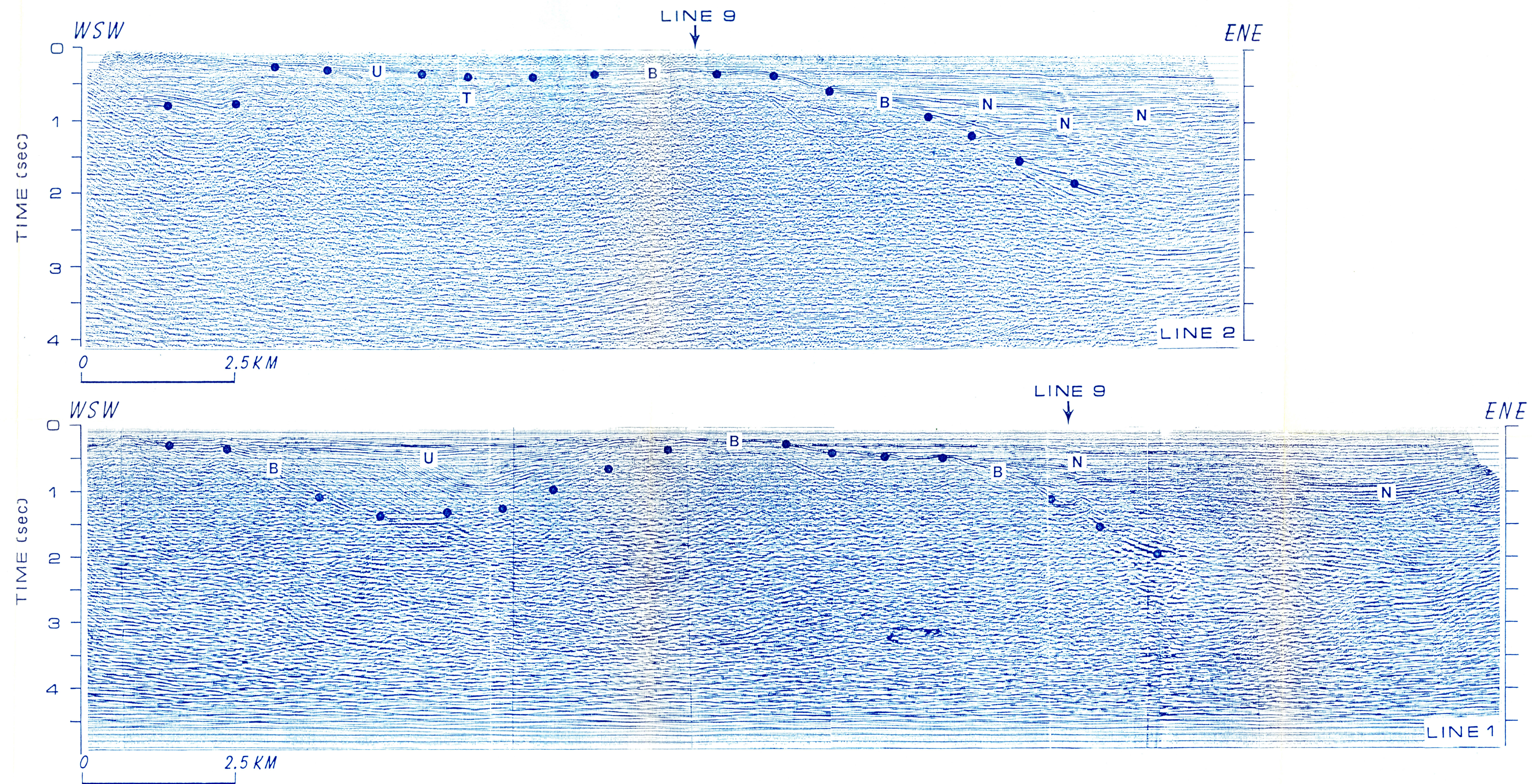
Plate 1. Seismic reflection lines 1 (bottom) and 2 (top) with interpretation. Location of intersecting lines shown with an arrow. B = sediment-basement reflector, N = normal fault, T = thrust fault, U = unconformity. Dots indicate sediment-basement contact.
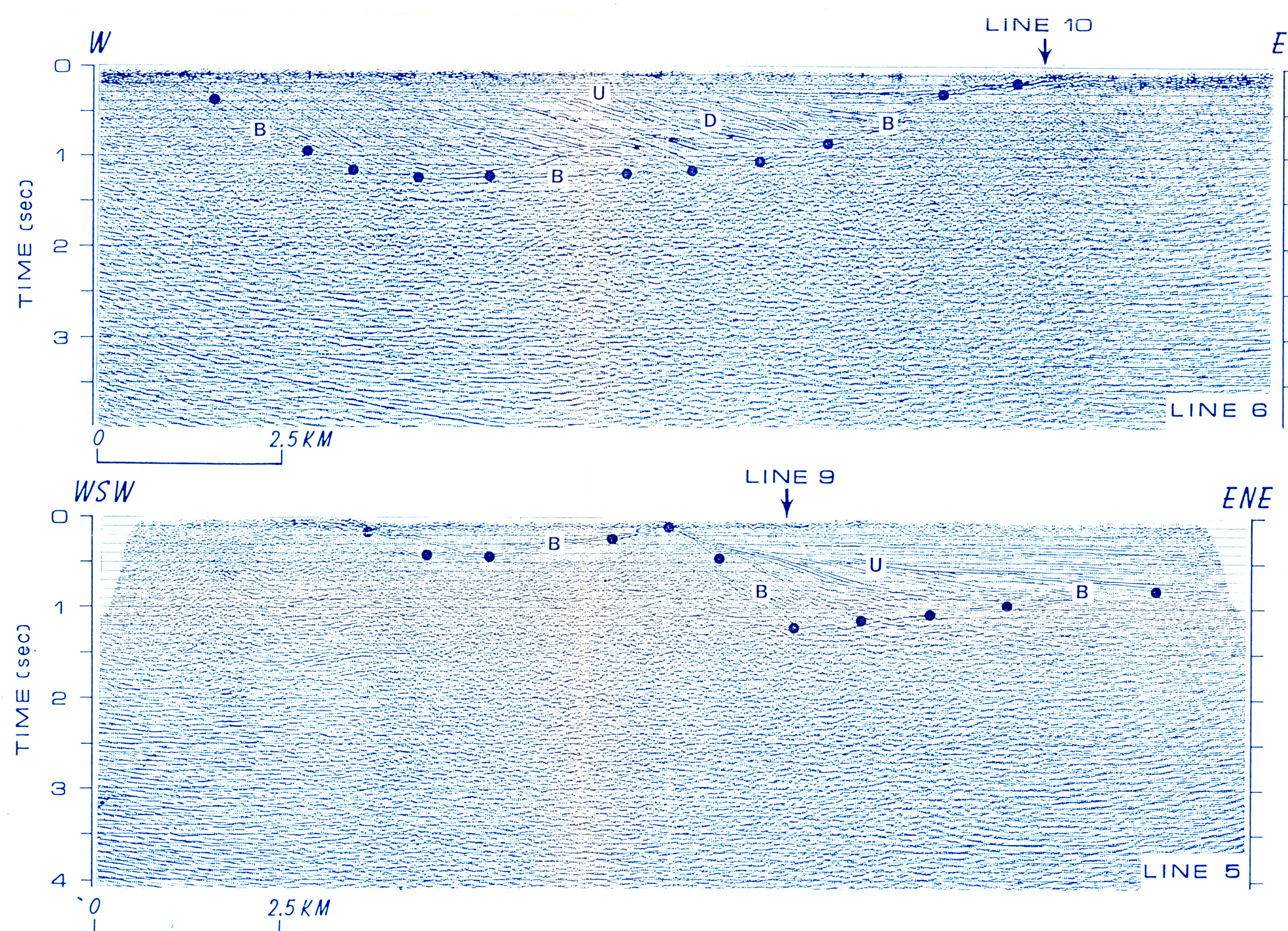
Plate 3. Seismic reflection lines 5 (bottom) and 6 (top) with interpretation. Location of intersecting lines shown with an arrow. B = sediment-basement reflector, U = unconformity, D = downlapping reflectors. Dots indicate sediment-basement contact.
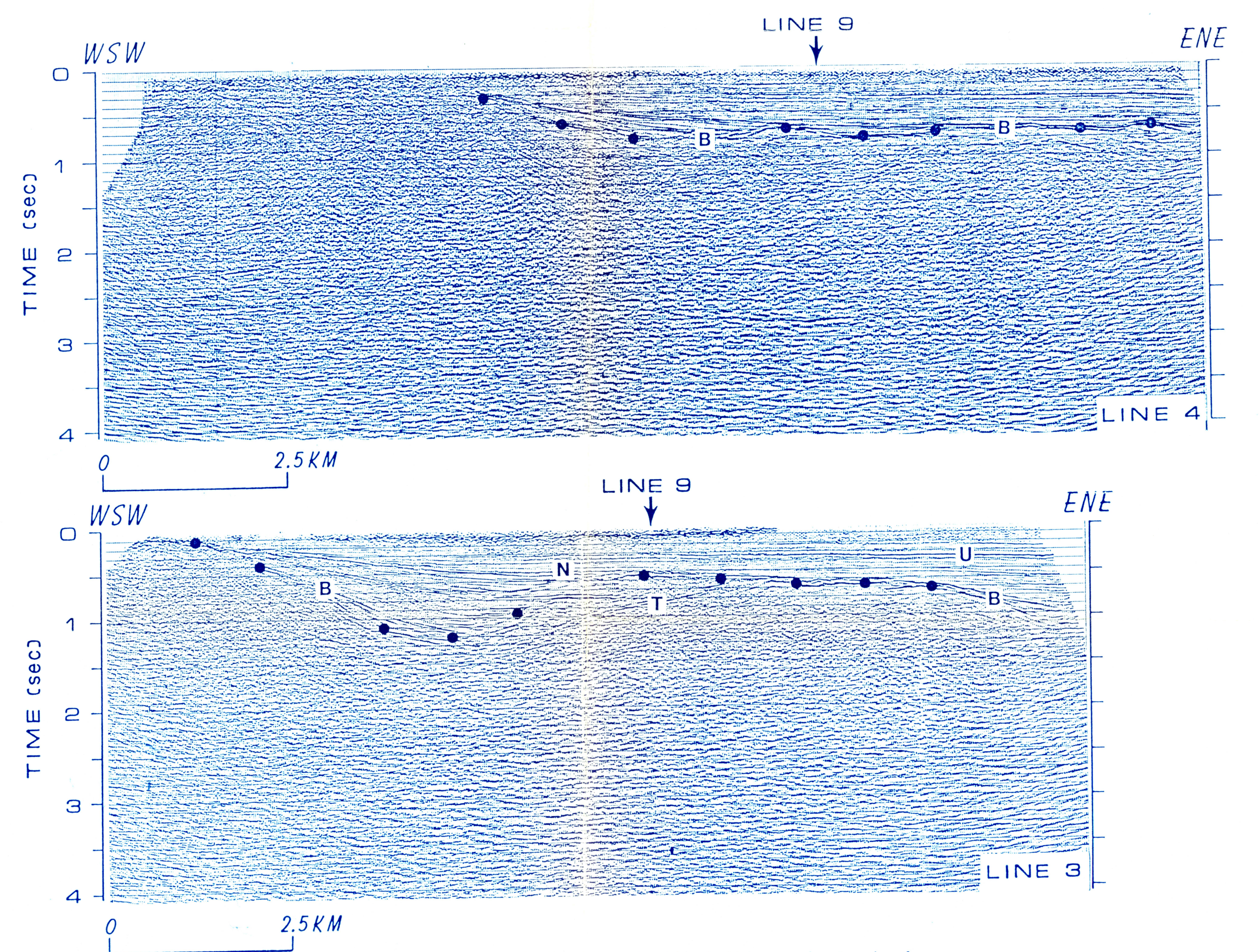
Plate 2. Seismic reflection lines 3 (bottom) and 4 (top) with interpretation. Location of intersecting lines shown with an arrow. B = sediment-basement reflector, N = normal fault, T = thrust fault, U = unconformity. Dots indicate sediment-basement contact.
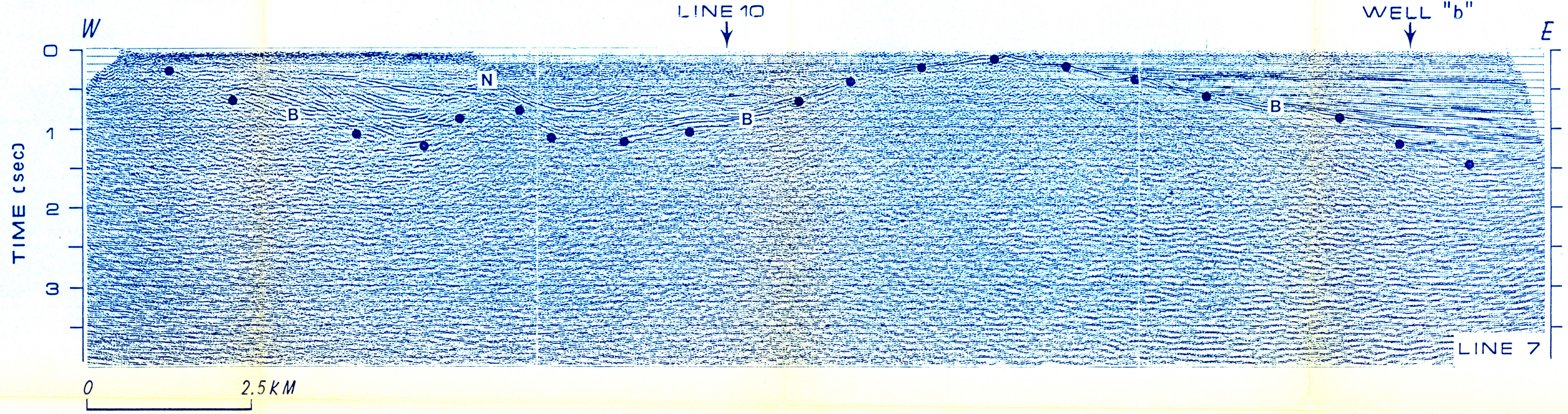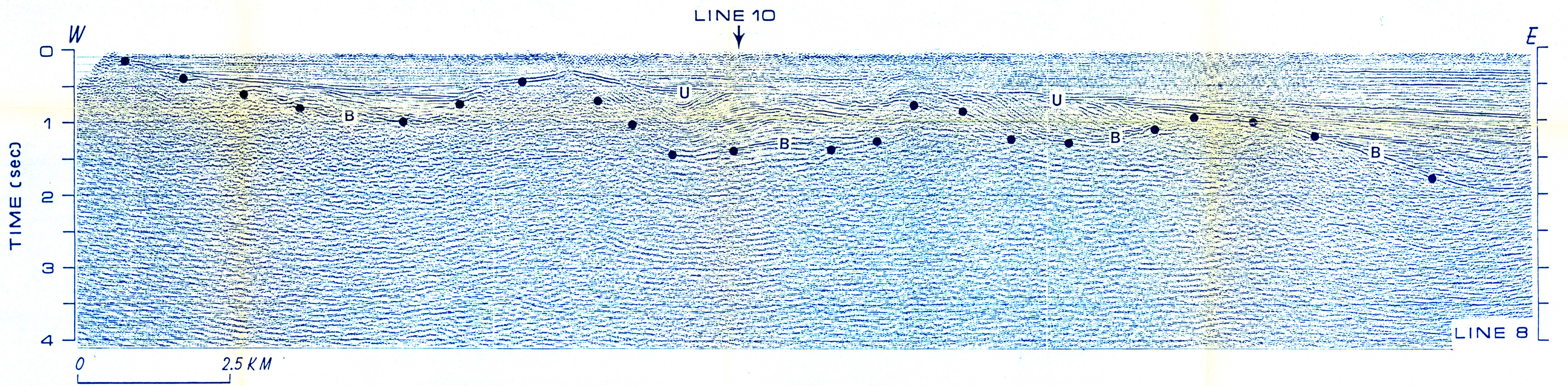
Plate 4. Seismic reflection lines 7 (bottom) and 8 (top) with interpretation. Location of
intersecting lines and Well "b" shown with an arrow. B = sediment-basement
reflector, N = normal fault, U = unconformity. Dots indicate sediment-
basement contact.
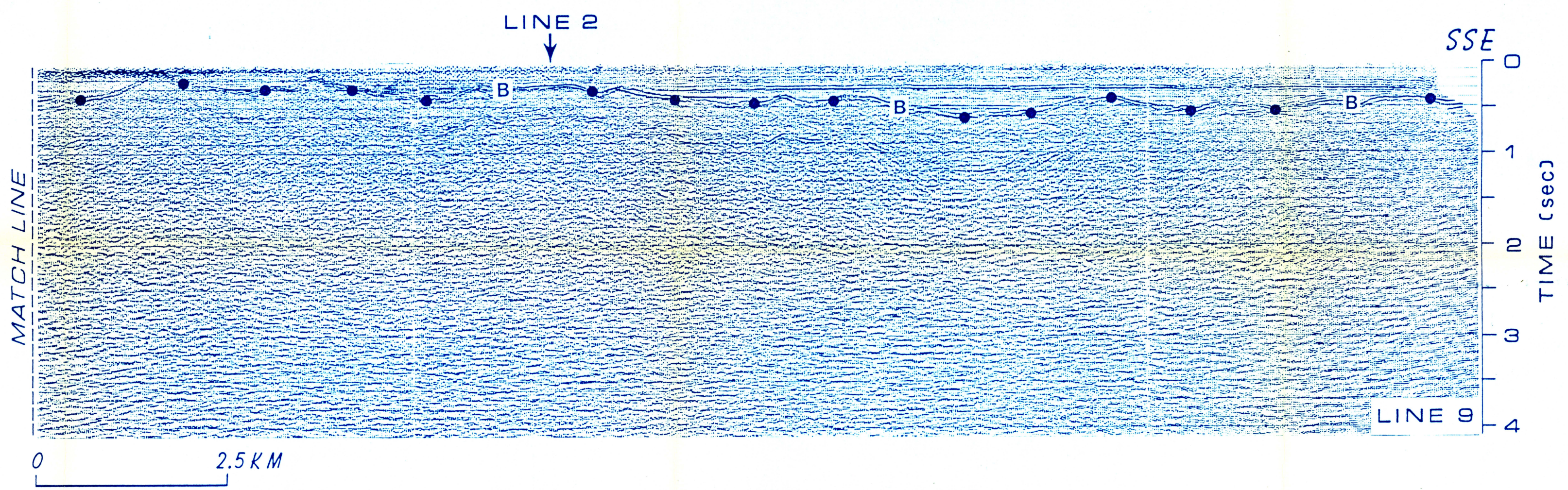
Plate 5. Seismic reflection Line 9 with interpretation. Location of intersecting lines shown
with an arrow. B = sediment-basement reflector, U = unconformity. Dots
indicate sediment-basement contact.
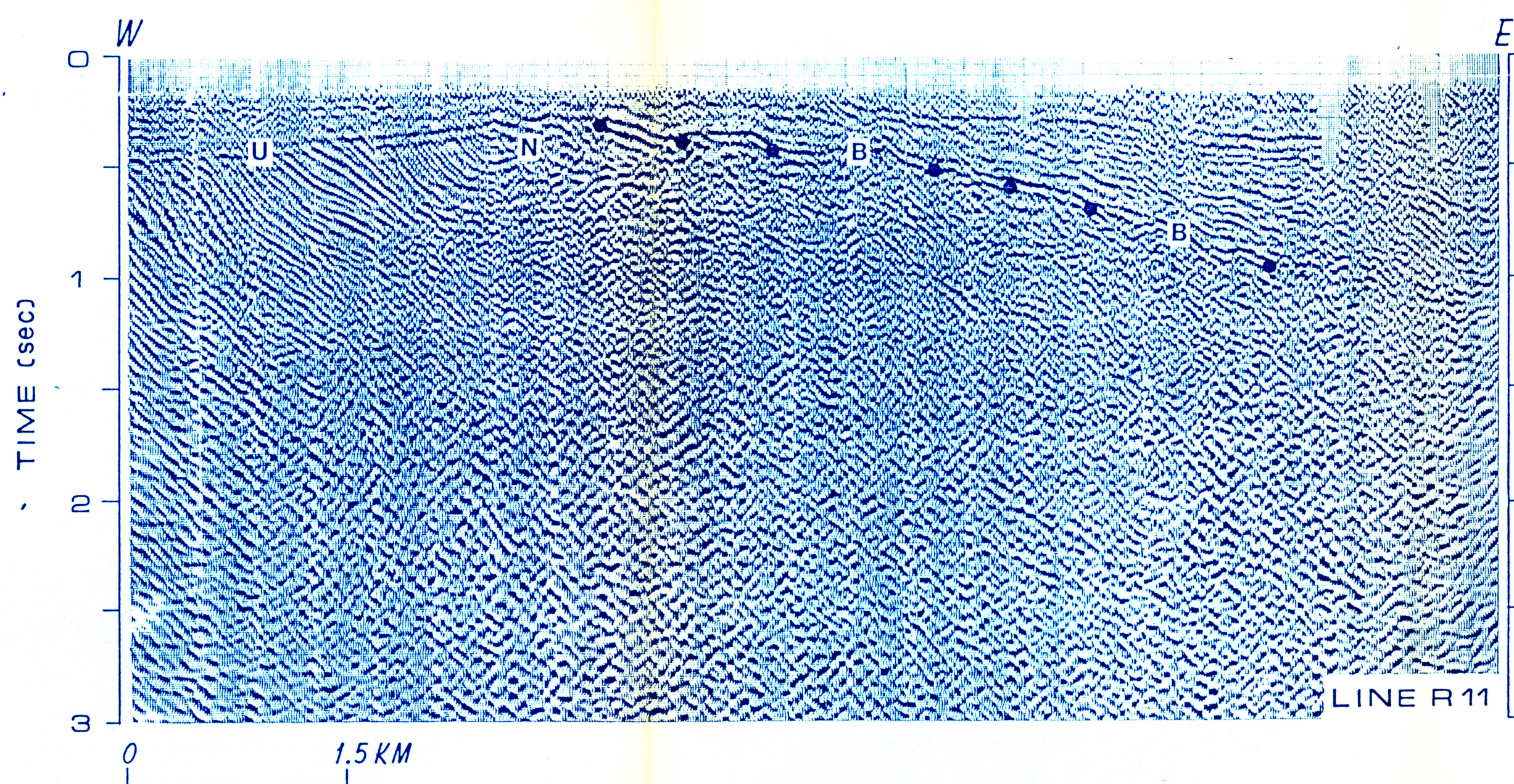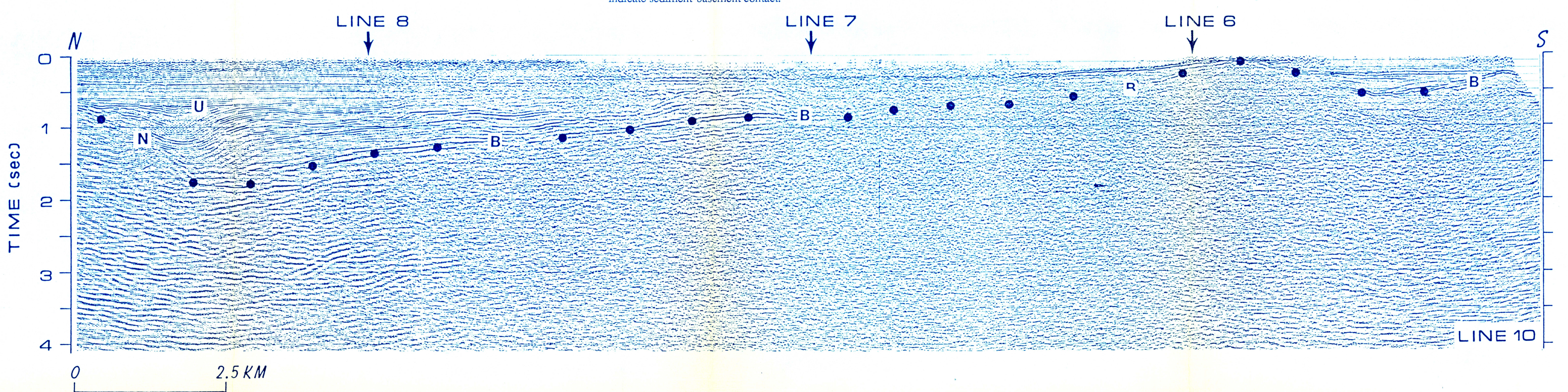
Plate 6. Seismic reflection lines R11 (bottom) and 10 (top) with interpretation.
Location of intersecting lines shown with an arrow. B = sediment-basement
reflector, N = normal fault, U = unconformity. Dots indicate sediment-
basement contact.